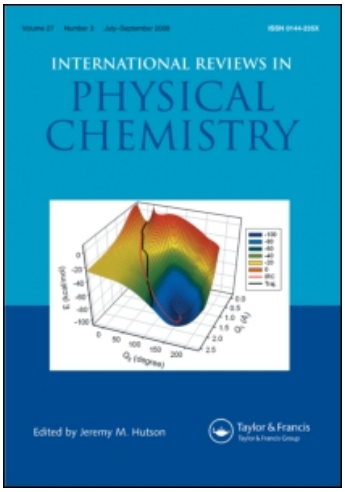

International Reviews in Physical Chemistry
Publication details, including instructions for authors and subscription information:
http://www.informaworld.com/smpp/title~content=t713724383

Controlling bond cleavage and probing intramolecular dynamics via photodissociation of rovibrationally excited molecules

Ilana Bar; Salman Rosenwaks

Online publication date: 26 November 2010

To cite this Article Bar, Ilana and Rosenwaks, Salman(2001) 'Controlling bond cleavage and probing intramolecular dynamics via photodissociation of rovibrationally excited molecules', International Reviews in Physical Chemistry, 20: 4, 711 — 749
To link to this Article: DOI: 10.1080/01442350110076484
URL: http://dx.doi.org/10.1080/01442350110076484

INT. REVIEWS IN PHYSICAL CHEMISTRY, 2001, VOL. 20, NO. 4, 711–749

Controlling bond cleavage and probing intramolecular dynamics via photodissociation of rovibrationally excited molecules

ILANA BAR*

The Institutes for Applied Research, Ben-Gurion University of the Negev, Beer-Sheva 84105, Israel

and SALMAN ROSENWAKS

Department of Physics, Ben-Gurion University of the Negev, Beer-Sheva 84105, Israel

Photodissociation studies of vibrationless ground state molecules pervade diverse areas of chemical physics, while those of rovibrationally excited molecules are expected to have even more impact due to the additional fascinating possibilities they offer and the new horizons they open. Photodissociation of rovibrationally excited species involves a double-resonance scheme in which a photodissociative transition is initiated from an excited rovibrational state that might substantially affect the intensity and wavelength dependence of the photoabsorption spectrum. In favourable cases, when the energy is disposed in vibrations that are strongly coupled to the reaction coordinate, this pre-excitation might influence photodissociation pathways and lead to selective bond cleavage. In other cases it might influence the branching ratio between different fragments by altering the photodissociation dynamics. Moreover, the photodissociation of rovibrationally excited species can serve as a sensitive means for detection of weak vibrational overtone transitions of jet-cooled molecules, and therefore a promising way for revealing specific couplings and time evolution of the prepared vibrational states. Experimental studies on different polyatomics are used to demonstrate the above aspects and to show how the mechanism of chemical transformations and the nature of rovibrationally excited states are highlighted by photolysis of these pre-excited molecules.

Contents

*Author for correspondence; e-mail: ibar@bgumail.bgu.ac.il

International Reviews in Physical Chemistry ISSN 0144–235X print/ISSN 1366–591X online © 2001 Taylor & Francis Ltd
http://www.tandf.co.uk/journals
DOI: 10.1080/01442350110076484

1. Introduction

Understanding the mechanism of reactions of polyatomic molecules, where bonds are formed or cleaved, is a long-standing goal and a most challenging target of chemical dynamics [1, 2]. Photodissociation is a particular means for bond cleavage attained by light activation and excitation of molecules to excited dissociative states, where one or more bonds are broken, provided that the light energy exceeds that of the weakest bond. Investigations of bond rupture are particularly promising since they unravel the dynamics of unimolecular chemical transformations and deepen our understanding in a wide variety of phenomena [1–8].

Photodissociation studies have greatly expanded due to the development of pulsed laser sources providing high power, spectrally narrow and temporally short pulses, polarization and tunability over a substantial portion of the electromagnetic spectrum. They also gained from the implementation of molecular beams, where cooling due to expansion decreases the population in all but several internal energy states, enabling better specification of the internal energy of the molecules. In particular, they received considerable stimulus from introduction of various techniques and sophisticated spectroscopic methods that rely on laser tunability and enable product state distribution to be determined. These methods [3] include laser-induced fluorescence (LIF), resonantly enhanced multiphoton ionization (REMPI), H-Rydberg time-of-flight (HRTOF), coherent anti-Stokes Raman scattering (CARS), time-resolved Fourier transform emission spectroscopy, chemiluminescence, photofragment imaging, time-of-flight mass spectrometry (TOFMS) and photofragment translational spectroscopy (PTS).

Bond breaking is investigated by initiating the photochemical decomposition and consequently interrogating the identity, the quantum specific states, the energy disposal and the vector correlations of the ensuing photofragments, using the above-mentioned methods. The results of these measurements disclose the detailed motion during the bond rupture step; further, they also address diverse areas of chemical physics of relevance to environmental chemistry, cluster and gas–surface phenomena and quantum scattering theory [1–8].

In vibrationally mediated photodissociation (VMP) [9–11], a variant of photodissociation, the excitation to the dissociative upper state is achieved via a double-resonance scheme, where the intermediate state is an individually prepared rovibrational state. VMP may have profound implications similar to photodissociation of vibrationless ground state molecules, but it is also of practical and fundamental significance due to the role vibrational energy plays in promoting chemical processes. From a practical point of view, vibrationally excited molecules are involved in many chemical processes, including those encountered in atmospheric, combustion and plasma systems, as well as in other domains ranging from laser operation to light-induced reactions and to energetic species used for surface etching [12]. Consequently, revealing the effect of vibrational excitation on reactivity

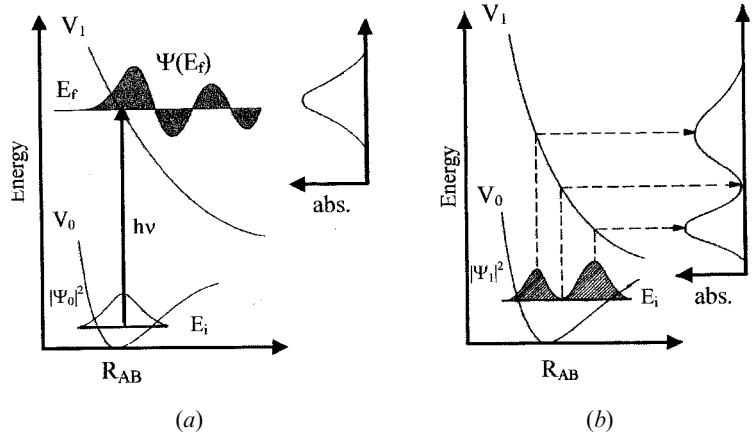

Figure 1. Schematic representation of potential curves and the corresponding absorption spectra of the parent molecule: (*a*) absorption from a vibrationless ground state to a directly dissociative potential energy surface (PES) consists of a broad continuum, and (*b*) absorption from a vibrationally excited state shows that promotion of extended regions on the ground state onto the dissociative PES are reflected in the absorption spectrum.

is essential to the understanding and characterization of the chemical and physical processes in many environments. From a theoretical perspective, exploring how vibrational excitation affects reaction dynamics and correlating the findings with the topology of the potential energy surface (PES) have long been of interest [1].

The vibrational pre-excitation may affect several intramolecular properties, since the vibrationally excited molecules may spend a great deal of their time sampling parts of the PES where their structure is different from that of their equilibrium geometry. Figure 1 illustrates schematically direct dissociation from the vibrationless ground state (*a*) and photodissociation from an intermediate vibrationally excited state (*b*). The former is characterized by a broad structureless absorption spectrum of the parent molecule, due to the reflection of the vibrationless ground state wavefunction on the upper PES, inversely proportional to the dissociation lifetime which is on the time-scale of the vibrational period (10^{-13} s). The latter is characterized by a spectrum that is the consequence of the reflection of extended regions on the ground state PES onto the dissociative upper state [2]. As clearly seen from figure 1, when the dissociation is promoted from a vibrationally excited state, different regions of the repulsive excited state are accessed as compared with those from the vibrationless ground state. It has to be recalled that indirect dissociation, termed as predissociation, also may occur. In the case where the excited state has a potential well, giving rise to a long-lived state and to dissociation from it through interaction with the dissociation continuum belonging to another electronic state, we encounter electronic predissociaton. In addition, in case of overlap of higher vibrational levels of an electronic state, or rotational levels of a given vibrational level with the dissociation continuum, vibrational or rotational predissociation takes place. Therefore, predissociation occurs on a slower time-scale and leads to a structured spectrum with broadened lines [13].

In VMP, preparation of an initial state that extends the amplitudes of the internal motion and survives long enough to interact with a photon may control the outcome

of the interaction. This might happen when the energy is disposed in vibrations that are strongly coupled to the reaction coordinate, providing selective access to distinct portions of the excited PES. It may thus facilitate design of reactions that lead to state-influenced or controlled photodissociation pathways and to predetermined outcome. The selective access may rise from preferential Franck–Condon (FC) overlap (the integral between the vibrational wavefunction of the initially prepared state and the wavefunction in the upper excited state). In other cases, owing to the participation of more than one excited PES, the different access of the upper PESs might lead to adiabatic and non-adiabatic processes resulting in different photodissociation pathways and influencing the branching ratio between different fragments by altering the photodissociation dynamics.

Of considerable importance, in its own right, is the possibility of gaining detailed understanding of the factors that control chemical reaction dynamics. The main problem in achieving reaction control is the difficulty encountered in preparation of states that resemble the reaction coordinate and their excitation is initially bond-localized. This is due to intramolecular vibrational redistribution (IVR) which causes the excitation to spread quickly and in an apparently complex manner over the entire molecular framework [14–17]. Usually a vibrationally excited molecular eigenstate, $|n\rangle$, is prepared, which is a linear combination of a zero-order bright state (ZOBS), $|s\rangle$, that interacts with a set of zero-order dark states $\{|l\rangle\}$ [18]:

$$|n\rangle = C_s^n|s\rangle + \Sigma C_l^n|l\rangle. \quad (1)$$

The ZOBS has the largest transition probability from the ground state to any of the zero-order states in a specified energy region. Therefore, if the eigenstate $|n\rangle$ contains a relatively high fraction of the ZOBS, it would be relatively easily prepared and supposing it resembles the reaction coordinate it also might drive the reaction well.

The zero-order states are usually described in terms of the normal mode (NM) [13] or the local mode (LM) model [19–21]. In the former, a vibrational mode is one in which all the nuclei of a molecule undergo harmonic motion, a representation that inherently comprises coupling among the bonds in a molecule. Producing a better NM description of the vibrational states in molecules requires addition of the anharmonicity. The LM model represents motions of individual anharmonic bonds and thus naturally includes anharmonicity, but not coupling between bonds, and therefore inclusion of interbond coupling is necessary to attain a better description. Both models intend to describe the vibrational states of molecules. Typically, the NM model accounts well for low vibrational states, while the LM for modes localized in a particular group of atoms. In particular, X-H (X = C, N or O) overtones of stretching vibrations are better understood in terms of the LM model, owing to their relatively small couplings to other bonds.

Understanding the mechanism of coupling of the ZOBS with other modes can be greatly aided by the exploitation of cooled samples in supersonic expansion in VMP studies followed by monitoring vibrational overtone spectra in which the spectral congestion is reduced extensively. Usually, other spectroscopic methods are quite limited in their ability to measure high overtone spectra of cold molecules, owing to a decrease in absorption cross-section of approximately one order of magnitude for each additional vibrational quantum number [14]. However, monitoring of action spectra, that is the photoproducts' yield as a function of the excitation laser wavelength in photolysis of rovibrationally excited molecules, can trace overtone

spectra effectively. The appearance of the bands is assisted often by the enhancement provided by better FC overlap of the initially prepared state and the upper excited state. Therefore, monitoring of action spectra by VMP offers several advantages. It provides sufficient sensitivity to detect vibrational excitation in molecules at the low density of supersonic expansion. In addition, for complex molecules, even the population in low energy vibrational modes is minimized at the relatively low vibrational temperatures of molecules in the supersonic expansion, reducing the contribution of hot bands usually overlapping the overtone spectral regions, and narrowing the observed spectra. Also, owing to the effective rotational cooling in supersonic expansion, several rotational states only are populated, leading to less congestion and extra narrowing and simplification of the spectrum. This narrowing allows one to distinguish between homogeneous and inhomogeneous broadening and to obtain upper limits for the former. The evaluation of the upper limits for the homogeneous linewidths enables the time-scale for the energy flow from the prepared state to be estimated. One more advantage is the possibility of observing new features that are otherwise overlaid by the excited band. Perceiving these features, related to intensity borrowing from the ZOBS, enables determination of specific couplings and of molecular constants, and estimates of time-scales for energy flow in the molecular frame.

This paper presents a survey of VMP studies, with particular emphasis on molecular systems with which the authors have been involved. The discussed examples illustrate the kinds of experiment and the type of information that can be realized from VMP experiments and the power of the approach. The survey starts with a description of the initial studies in the field and proceeds with the simplest polyatomic system, the heteronuclear triatomic prototype, that is water isotopomers, a benchmark of many VMP studies performed by different research groups. Then we proceed to molecules possessing four atoms, with particular focus on acetylene isotopomers and finally to even larger systems including propyne, a homologue of acetylene, and methane and ethane derivatives of hydrochlorofluorocarbons (HCFCs). It is shown that by measuring the identity or state distribution of different photofragments the dynamics of the processes may be revealed.

2. Experimental approach

The concept behind VMP experiments, shown in figure 2, comprises three steps: preparation of a well-defined eigenstate, interaction of this state with ultraviolet (UV) photons which promote it to upper PES(s) where it decomposes, and finally interrogation of the ensuing photofragments. The described experimental procedure provides a unique fashion for testing the connection between the preparation of the initial rovibrational state and the resulting different dissociation pathways that might affect the identities and state distributions of the photofragments.

2.1. *Rovibrational excitation*

The rovibrational preparation is accomplished by direct optical (infrared (IR) or visible (VIS)) excitation or stimulated Raman excitation (SRE). In optical excitation, one photon, of the proper frequency, directly excites fundamentals or hot bands as well as vibrational overtones and combination bands. IR vibrational transitions are strongly allowed when $\Delta v = \pm 1$ [13] (inducing efficient excitation of fundamentals or hot bands). Excitation to higher vibrational states is possible due to mechanical and

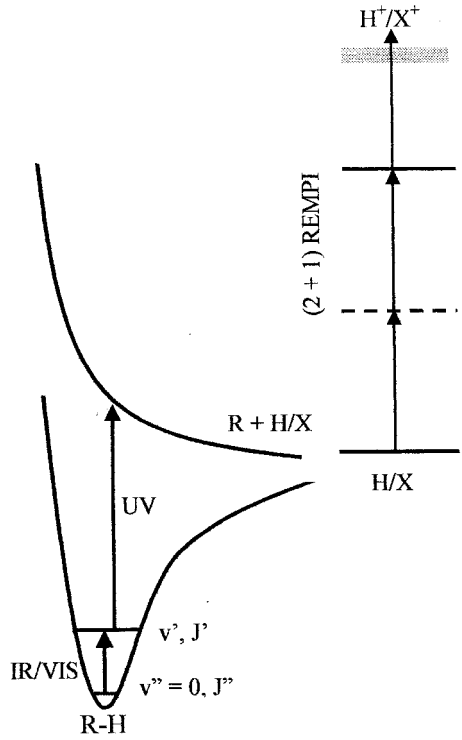

Figure 2. A schematic description of the concept of vibrationally mediated photodissociation studies. It encompasses three steps: excitation of a well-defined eigenstate, its interaction with UV photons, which promote the molecule to upper PES(s) where it decomposes, and finally tagging of the ensuing photofragments.

electrical anharmonicities relaxing the vibrational selection rules, but the transition probabilities to vibrational overtones and combination bands are weak and they are harder to excite [14]. The intensities of these transitions are exponentially decreasing functions of the total change of the vibrational quantum number, Δv, decreasing by a factor of about 10 for each quantum of excitation. Consequently, in a given spectral interval the most efficient transition from the ground state is to the lowest Δv and highest anharmonicity, meaning that hydride stretches are those that can be most efficiently excited. In our experiments, IR/VIS photons were employed to excite C-H(D) or O-D overtones and combination bands of C-H stretches and bends of several molecules. These photons were provided by a Nd:YAG pumped tunable dye laser, by a Raman shifted Nd:YAG pumped tunable dye laser, or by an optical parametric oscillator (OPO) pumped by the third harmonics of a Nd:YAG, depending on the excited state, the required frequency and the available laser source at the time of experiment. The laser pulses employed for the vibrational excitation were of about 6 ns duration, of bandwidth about $0.08\,cm^{-1}$ and of energies from several millijoules to several tens of millijoules.

In SRE the molecule can be excited to fundamental or low overtones via interaction with two laser beams at frequencies ω_p (pump) and ω_S (Stokes), with a difference frequency $(\omega_p - \omega_S)$ resonant with a Raman transition. In our experiments, ω_S came from a Nd:YAG pumped tunable dye laser and ω_p from the doubled

residual of the Nd:YAG first harmonic. The selection rules for the SRE process differ from those for direct one-photon excitation [13], leading to access of symmetric stretches or bends. The states that we prepared by SRE include hydride fundamental stretches (O–H(D) or C–H) of the above-mentioned molecules.

Measurements of rovibrational spectra enable detection of the excitation. CARS [22, 23] or photoacoustic Raman spectroscopy (PARS) [24] were employed to monitor SRE by tuning the Stokes laser across the rovibrational transitions. CARS is a four-wave mixing process, where the waves of frequencies ω_p, ω_S, ω_p are mixed in a sample to generate a new coherent wave at frequency $\omega_{AS} = \omega_p - \omega_S + \omega_p$ (ω_{AS} is the anti-Stokes beam). In PARS, the nonlinear process occurring in SRE results in amplification of ω_S and attenuation of ω_p. For each generated Stokes photon a molecule is transferred to a rovibrationally excited level. Rovibrational levels in direct optical excitation, where the IR/VIS laser was scanned across the rovibrational transitions, were monitored by photoacoustic (PA) spectroscopy [24]. Both PA spectroscopy and PARS detect the sound wave generated by vibrational relaxation of a sample, at a pressure of several up to hundreds of torrs, present in an auxiliary cell equipped with a tiny microphone.

Additional methods can be employed for depositing large amounts of energy in vibrational states of molecules. They include FC pumping to an excited electronic state followed by stimulated emission pumping (SEP) from this state to a high vibrational level of the ground electronic state [25], IR multiphoton excitation [26] and stimulated Raman adiabatic passage (STIRAP) [27]. The promotion of molecules in SEP is by two photons of different wavelengths and the reachable vibrational states correspond to quite different skeletal motions of the molecule than those accessible in direct excitation. SEP is used extensively as a spectroscopic method to provide new insights into IVR [14], but has not been employed as yet for pre-excitation of vibrational states in VMP studies. The IR multiphoton excitation approach includes absorption of IR photons delivered by an intense laser, and enables deposition of many quanta of vibrational excitation with quite high efficiency but low specificity. STIRAP uses partially overlapping pulses (of pump and Stokes lasers) to produce highly efficient population transfer between quantum states of an atom or a molecule. The procedure relies on an initial creation of coherence with subsequent adiabatic evolution. However, STIRAP has limitations for excitation of polyatomics, since in case of increased density of levels, particular transitions possess substantially smaller line strength, requiring adequate laser power to achieve efficient transfer in polyatomics [27]. It has to be pointed out that like SEP, both IR multiphoton excitation and STIRAP have not been used as yet in VMP studies.

2.2. *Photodissociation*

The wavelength of the photodissociating (UV) photon is chosen to be at the leading edge of the absorption band of the molecule. Therefore, the photon energy is insufficient to induce effectively the dissociation of vibrationless ground state molecules and the background due to this process is small. Pre-excitation of a fundamental or overtone vibration leads to enhanced absorption of the UV photon, particularly when the FC factors are favourable, and thus to efficient photodissociation.

Consequently, photodissociation of pre-excited water isotopomers was performed by 193 nm UV photons, provided by an ArF excimer laser, that of

vibrationally excited acetylene isotopomers and propyne by about 243 nm photons and of HCFCs by about 243 or about 235 nm photons. The about 243 and about 235 nm wavelengths were supplied by the doubled output of a Nd:YAG pumped dye laser. These photons were selected to induce effective absorption only when pre-excited molecules were available and to fit the wavelengths of the corresponding two-photon REMPI transitions employed for tagging the emerging photofragments.

2.3. *Photofragment detection*

The emerging photofragments were detected by LIF, or alternatively, by $(2+1)$ REMPI [28]. LIF detection requires a suitable electronic transition for the fragments of interest, accessible with a pulsed dye laser through one- or two-photon transition, and well-characterized spectroscopy of the corresponding transition. REMPI involves state-selective ionization of neutral fragments, at the place they are born, via an intermediate state. $(2+1)$ REMPI involves two-photon excitation to the intermediate resonant state and an additional photon of the same colour for photofragment ionization. The advantage of REMPI, when coupled with a mass spectrometer, is that it affords not only fragment detection, but also mass selective spectra that can differentiate between isotopomers. We employed LIF to interrogate OH(OD) radicals, released as a result of VMP of water isotopomers, on the A, $^2\Sigma^+ v' = 0, 1 \quad \mathrm{X}, ^2\Pi\, v'' = 0$ transitions at about 307 or 283 nm [29].

REMPI was applied for detection of H(D) ejected in VMP of acetylene isotopomers, propyne and HCFCs. For HCFCs, also chlorine photofragments in their ground (Cl) and spin-orbit excited states (Cl*) were monitored. The photofragments were detected by the following two-photon transitions: H(D) $(2s\ ^2S \quad 1s\ ^2S)$ at 243.135 (243.069) nm [30], Cl $(4p\ ^2D_{3/2} \quad 3p\ ^2P_{3/2})$ at 235.336 nm [30] and Cl* $(4p\ ^2P_{1/2} \quad 3p\ ^2P_{1/2})$ at 235.205 nm [31]. The wavelengths for the LIF/REMPI detection were provided by the doubled tunable output of a XeCl excimer or Nd:YAG pumped dye laser. The laser pulses were of about 16 or about 6 ns duration respectively and of about $0.5\,\mathrm{cm}^{-1}$ bandwidth. Pulses of 130 μJ were used to minimize two-photon absorption in the photodissociating step and to prevent saturation of the REMPI. Pulses of about 7 μJ were used to minimize saturation of the OH(OD) transitions in the water experiments.

The water isotopomers were flowed into a gas cell at low pressure, in the range of several hundreds of millitorr, to reduce collisions of the ensuing photofragments. The REMPI detection was conducted in a home-built Wiley–McLaren TOFMS [32] which provided sensitive and mass-selective detection. The ions formed via REMPI were subject to continuously biased extraction, two acceleration stages, two pairs of orthogonal deflection plates and an Einzel lens prior to entering the field-free drift region and eventual detection by a microsphere plate. The sample was introduced in the TOFMS chamber via a pulsed valve-needle or valve-skimmer arrangement, enabling cooling of the molecules. Some of the samples were of neat compounds, while others seeded in Ar and the sample pressure, in the chamber, was in the range of $5 \times 10^{-6} - 2 \times 10^{-5}$ Torr. The IR/VIS and UV beams counterpropagated and entered the chamber perpendicularly to both the TOFMS axis and the molecular beam axis. They were introduced collinearly to a common focus in the centre of the ionization region of the TOFMS. The delay between the IR/VIS and UV pulses was in the range of 10–20 ns.

2.4. *Types of measurement*

The measurements intended to probe the dynamics of bond rupture by establishing the effect of vibrational excitation on the branching among different photofragments or on the state distribution of the ensuing photofragments. The experimental system facilitated generation of action spectra, Doppler profiles and TOF profiles or mass spectra (MS). Action spectra monitor the yield of the photoproducts as a function of the exciting laser (Stokes or IR/VIS) wavelength due to photolysis of rovibrationally excited molecules, while keeping the photodissociating and probe laser wavelengths fixed. Tuning the vibrational overtone excitation laser to a particular rovibrational transition of the molecule and varying the probe laser wavelength, the OH(OD) quantum state distribution or the Doppler profiles of the OH, H(D) or Cl and Cl* photofragments were monitored. Measuring the Doppler profiles of the atomic fragments and taking into account the transition probabilities and the integrated areas under the profiles, enabled extraction of the branching ratios into the different photodissociation channels. In addition, these profiles allowed extraction of the translational energies of the photofragments. The TOF profiles and MS were monitored when the UV laser was fixed on the electronic transition and the IR/VIS lasers on the rovibrational transitions and the dependence of the intensity of the REMPI signal on time was acquired. In addition, using polarized laser beams, LIF/Doppler broadened spectral line shapes and REMPI/time-of-arrival profiles were measured. These profiles afforded extraction of vector correlations [33–37], particularly between the transition dipole moment $\boldsymbol{\mu}$ in the parent molecule, the velocity $\mathbf{v}$ and the angular momentum $\mathbf{J}$ of the recoiling photofragment, enabling a most detailed insight into the dynamics of some VMP processes.

3. Photodissociation of pre-excited molecules

We have already alluded to the merits of VMP explorations, however, only explicit description of examples can highlight and illustrate the wealth of detailed insight that can be gained by VMP.

3.1. *In the beginning*

In the late 1970s and the early 1980s theoretical and experimental groups both raised the interest in effects induced by vibrational excitation in triatomics. These molecules were selected as attractive objects since they are small enough to allow *ab initio* calculations of PESs and photodynamics and yet possess several vibrational degrees of freedom, such as stretches and bends, which play a principal role also in larger molecules. Different methods were used to calculate state-to-state photodissociation cross-sections from vibrationally excited states for a number of molecules, including HCN and DCN [38], N_2O [39] and O_3 [40]. Experiments aimed at measurement of the same effect using initial laser excitation to a particular vibrational state (fundamentals or first overtone of bendings) followed by probing of the resulting photoabsorption or photodissociation spectra, were carried out in O_3 [41, 42], OCS [43] and CH_3Br [44]. These experiments used fixed frequency molecular lasers or line-tuned CO_2 lasers to excite vibrational modes of the molecules, followed by UV photolysis to dissociate them. Taking advantage of the change in cross-sections as a result of vibrational excitation, by factors of several hundreds, and of the coincidence of laser wavelengths with specific absorption lines of isotopes,

enabled isotope separation. Usually, these experiments were carried out on mixtures of the investigated compound and another molecule that scavenged the photogenerated atoms. Following accumulation of the products of many pulses they were analysed mass spectrometrically to determine the relative photodissociation yields. Also, an additional approach measured the temperature dependence of photoabsorption spectra and extracted the components related to the contributions of the populated low energy vibrational states in O_3 [42] and OCS [45]. This method is less specific, because with increasing temperature many vibrationally excited states are populated, complicating the direct extraction of the contribution of the different states.

In another set of experiments, molecules containing substantial vibrational energy, four to six quanta of O-H stretch, including hydrogen peroxide (HOOH) [46], nitric acid ($HONO_2$) [47], and *tert*-butyl hydroperoxide ($(CH_3)_3COOH$) [48], were photodissociated. In these experiments the O-H excitation energy was intramolecularly coupled into the O-O or O-N stretch that became the cleaved bond and they particularly emphasized the comparison of product state distribution from VMP to those from an isoenergetic single photon photolysis.

Nevertheless, the cornerstone to a new era of state-to-state studies probing the population of individual states of ensuing photofragments and enabling crucial comparison with theory were the innovative studies of H_2O [2, 8, 49]. Particular rovibrational states in the antisymmetric stretch of water were prepared by Raman shifted photons from a dye laser. These states were then photodissociated by a 193 nm laser beam followed by a UV beam, from a frequency doubled dye laser, for OH photofragment LIF tagging. From the resulting spectra, OH rotational distributions were extracted showing their sensitive dependence on the parent state and excellent agreement with the results of a simple FC model which included the rotational and electronic degrees of freedom. These findings have spurred both theoretical and experimental activity on water and its isotopomers, opening the arena of state-resolved studies and particularly of controlling photodissociation pathways by VMP.

3.2. *Water isotopomers*

Theoretical predictions on bond selectivity in HOD, in the second ($\tilde{\mathbf{B}}\ ^1A_1 \quad \tilde{\mathbf{X}}\ ^1A_1$) [50] and in the first absorption band ($\tilde{\mathbf{A}}\ ^1B_1 \quad \tilde{\mathbf{X}}\ ^1A_1$) [51, 52], attracted attention to the possibility of controlling product identity via VMP. The photodissociation of water in the first absorption band was considered as a fast and direct bond breaking process on a single PES. The quantum mechanical time-independent [51] and time-dependent dynamics calculations [52] mostly used a semiempirical ground state PES [53] and an *ab initio* $\tilde{\mathbf{A}}$ state surface [54]. These studies predicted isotopic branching ratios for the photodissociation, via two distinguishable channels leading to $HOD \rightarrow OD + H$ ($OH + D$) with small energetic differences originating from the different zero-point energies of O-H and O-D. The calculations showed that these ratios strongly depend on the frequency of the dissociating photon and the vibrational state out of which the photodissociation was initiated. Explicitly, the absorption curve of vibrationally excited HOD is red shifted relative to that of vibrationless ground state H_2O, HOD and D_2O. This affords almost exclusive production of $OD + H$ or $OH + D$ depending on the initial state from which the photodissociation was started and on the photolysing photon [52]. Moreover, the calculations anticipated selective production of $OD + H$ even for

low vibrational excitation, while of OH + D only when the photodissociation begins from HOD ($3\nu_{OD}$) and higher. The calculations led, already more than a decade ago, to experimental efforts on HOD photodissociation of excited O-H overtones [55], and O-H and O-D fundamentals [56].

In particular, it seemed that preparation of distinct initial vibrational eigenstates representing nearly pure O-H or O-D stretches and storing of vibrational energy exclusively in one bond or another of HOD, might be the most stringent test of reaction dynamics control. The first VMP experiment where two different vibrational states, O-H (about 3700 cm^{-1}) and O-D (about 2700 cm^{-1}) stretches, served as the intermediate states from which HOD was promoted to an upper electronic state was carried out in our laboratory [56]. In this experiment SRE was introduced to prepare rovibrationally excited HOD molecules and CARS to perceive their excitation. The SRE was followed by 193 nm photodissociation via the $\tilde{A}$ state and LIF interrogation of the OH(OD) photofragments in an attempt to understand and ultimately control the course of this reaction [56].

Tuning of the Stokes laser through the Q-branch transitions of HOD ($1\nu_{OH}$) enabled simultaneous monitoring of the CARS spectrum (figure 3(*a*)) and one of the reactant yield spectra, that is action spectra of OD (figure 3(*b*)) or OH (figure 3(*c*)). The latter spectra were monitored while keeping the wavelength of the probe laser constant on the $R_2(4)$ line of the A, $^2\Sigma^+$ $v' = 0$, X, $^2\Pi$ $v'' = 0$ transition of the OH or OD photofragments. Comparison of the action spectra to the CARS spectrum shows that the photodissociation of HOD molecules is enhanced whenever particular rotational states of the O-H stretch are prepared. From this enhancement and from the SRE rovibrational pumping efficiency, a about 300-fold increase in the 193 nm photodissociation cross-section of HOD ($1\nu_{OH}$) relative to that of vibrationless ground state water isotopomers (25% D_2O, 50% HOD and 25% H_2O present in the reaction mixture) was roughly estimated [56]. Moreover, the OD fluorescence intensity was higher than that of the OH, demonstrating that the 193 nm photodissociation of HOD ($1\nu_{OH}$) produced more OD than OH with a branching ratio of 2.5 ± 0.5. When similar measurements were conducted on HOD ($1\nu_{OD}$), a completely different behaviour was encountered. Even though the CARS signal (figure 3(*d*)), monitored when the SRE was tuned through the rotational levels of the HOD ($1\nu_{OD}$), seemed to be of almost similar intensity to that of $1\nu_{OH}$, neither the fluorescence of OD (figure 3(*e*)) nor OH (figure 3(*f*)) was enhanced. These measurements clearly demonstrate that excitation of even the lowest vibrational level of HOD has a dramatic effect on the photodissociation cross-section. This agrees with the theoretical predictions that the FC effects are the source of both the difference in photodissociation behaviour of HOD ($1\nu_{OH}$) and ($1\nu_{OD}$) and the selectivity in bond breaking of HOD ($1\nu_{OH}$). The enhancement of the photodissociation cross-section of HOD ($1\nu_{OH}$) is the result of a much better overlap of the dissociative continuum with the $1\nu_{OH}$ vibrational wavefunction than with either the vibrationless ground state or $1\nu_{OD}$. Although the vibrational excitation of the OD stretch in HOD ($1\nu_{OD}$) gives the O-D bond an initial 'push' in the direction of the dissociation coordinate to OH + D, the unfavourable FC factor precludes the enhancement of the dissociation. In contrast, in HOD ($1\nu_{OH}$), the favourable FC factors enabled the additional energy along the OD + H dissociation coordinate to be very effective at enhancing the dissociation. Thus, these factors were the source of bond selectivity in the fragmentation of HOD ($1\nu_{OH}$), owing to the better FC overlap of the prepared wavefunction with the OD + H continuum than with the

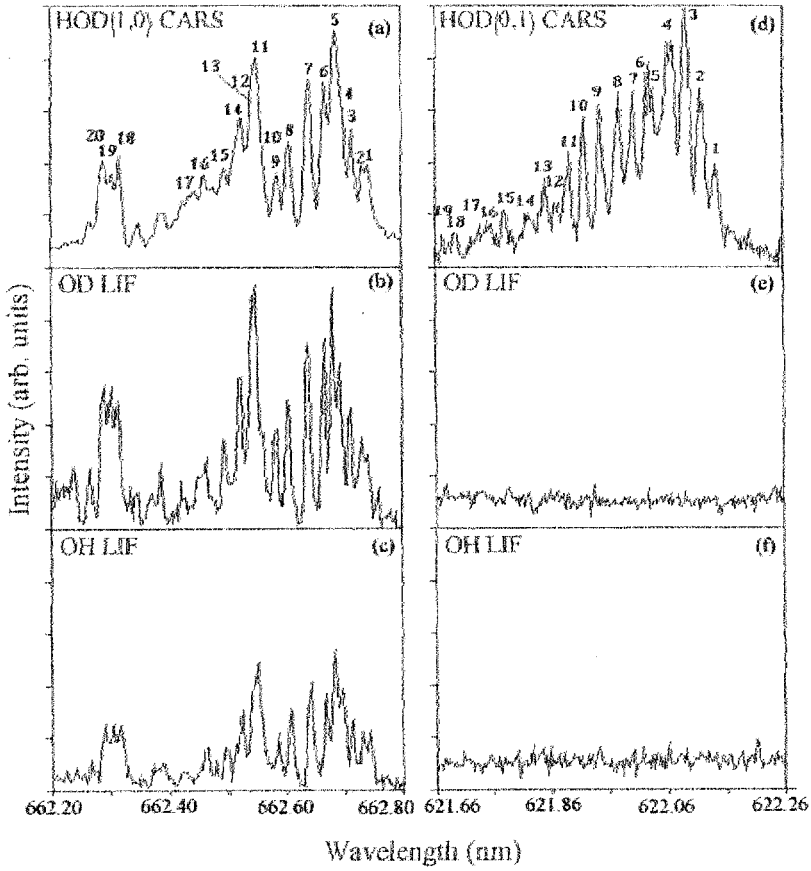

Figure 3. Excitation of HOD ($v''_{OH} = 1$) and ($v''_{OD} = 1$) performed by scanning of the Stokes beam via the rovibrational levels: (*a*) and (*d*) CARS signal, (*b*) and (*e*), and (*c*) and (*f*) LIF of the $R_2(4)$ line of A, $v' = 0$ X, $v'' = 0$ transition of the OD and OH photofragments, respectively. The intensity scale in (*b*) and (*c*) is similar. Reprinted with permission from Bar *et al.*, *J. chem. Phys.*, **93**, 2146, © 1990 American Institute of Physics and Bar *et al.*, *J. chem. Phys.*, **95**, 3341, © 1991 American Institute of Physics.

OH + D continuum [52, 56]. This VMP study, where two distinct states with a single quantum of vibrational excitation were prepared, confirmed that it is not enough to weaken the bond to be cleaved to obtain bond selectivity, but rather a preferential FC overlap of the vibrational wavefunction with the corresponding channel on the dissociative excited state is essential.

As mentioned above, fragmentation to OH + D is not easily achieved, but can be accomplished after a choice of a higher O-D stretch, greater than $3\nu_{OD}$, before the addition of the UV photon [52]. Indeed, direct excitation of $3\nu_{OD}$ by Raman shifted output of a dye laser, around 7960 cm^{-1}, followed by 193 nm photodissociation, directed the bond cleavage in favour of the OH + D channel, with a (OH + D)/(OD + H) branching ratio of 2.6 ± 0.5 [57]. Here as well, the origin of the selectivity is the favourable FC overlap that enables the additional rovibrational energy to effectively enhance the dissociation and particularly to be channelled along the OH + D channel. It is worth noting that the observed ratios agree only qualitatively with the calculated ones [52, 56, 57].

Realization of even larger selectivity was obtained in the VMP experiments on HOD from states containing four or five O-H quanta [55, 58]. These experiments showed enhancement of OD over OH or comparable amounts of the two, depending on the UV photon promoting the photodissociation [55]. VMP of $4\nu_{OH}$ photolysed by 266 nm photons formed at least 15-fold excess of OD, preferentially cleaving the O-H bond. Similar behaviour was encountered in the 239.5 nm photodissociation of $4\nu_{OH}$, but this behaviour changed dramatically for a still more energetic photon of 218.5 nm producing comparable amounts of OD and OH [55]. Again, the accessible regions on the upper electronic states were the keys to the dramatic change in the branching ratios for the different wavelengths. The two longer wavelength (266 and 239.5 nm) photons connected the vibrationally excited state to the electronically excited state only in regions well out in the exit channel for breaking the O-H bond, while for the shortest wavelength either bond was broken [9, 55]. The dominant OD + H channel was also apparent in the 288 nm photodissociation of rotational states selected in the third and fourth O-H stretching overtones of HOD, with a (OD + H)/(OH + D) ratio of greater than 23 for the higher overtone and of greater than 12 for the lower [58]. This indicates again that the selectivity was less pronounced for total energies that sample the barrier region for crossing between OH + D and H + OD on the excited $\tilde{A}$ surface. For total energies below the barrier, the enhancement of OD versus OH was improved by increased ν_{OH} vibrational excitation.

An additional point should be raised concerning the agreement between the measured (OD + H)/(OH + D) branching ratios and the quantum scattering calculations [47, 48]. In the VMP studies of $4\nu_{OH}$ and $5\nu_{OH}$ [55, 58] and in the 157 nm photolysis of ground state HOD [59] the agreement was very good. However, in the 193 nm photodissociation of $1\nu_{OH}$ [56] and $3\nu_{OD}$ [57] and ground state HOD [60], the measured ratios were smaller than expected, with less satisfying agreement. As recently suggested, it is likely that another mechanism, that primarily affects the photodissociation in the long wavelength region of the first absorption band of water, has to be considered [60, 61]. A possible explanation is that the contribution to the photodissociation in the long-wavelength region, that is the non-FC region, comes from both the singlet, $\tilde{A}\ ^1B_1$ state and the lowest triplet PES, $^3B_1$ [60, 61]. This indicates that even the photolysis of the benchmark molecule is not yet fully understood, in the red tail region of the absorption, and points to the importance of the interplay between theory and experiment to gain a better understanding.

Although the branching ratio into distinct product channels is of profound interest and contains a wealth of dynamical information on bond rupture, additional aspects related to the dependence of photodissociation dynamics on reagent states are important as well. The VMP that prepares rovibrational states on the ground electronic state and subsequently promotes them into the upper continuum affords studying photodissociation of water isotopomers on a truly state-to-state level. This way the effect of initial vibration and overall rotation of the reagent molecule on the vibrational and rotational distribution of the OH(OD) photofragment is revealed. Indeed, state-to-state studies on HOD [58], H_2O [49, 62–66] and D_2O [67] showed that initial vibrational and rotational motions affect the energy and vectorial disposal [68] in the OH (OD) photofragment. The state-to-state photodissociation at 193 nm of the fundamental symmetric stretch of water, H_2O (1, 0, 0), is one of the examples that demonstrate these findings [63, 68].

The rotational distribution of the OH resulting from photodissociation of H_2O (1, 0, 0) is structured, dependent on the particular rotation out of which the photodissociation is promoted [63], and its comparison to the FC model [49] shows reasonable agreement. It is worth noting that the predictions of the FC theory are for photolysis of selected rotational states of H_2O (0, 0, 1) [49]. However, these calculations consider the OH rotational distribution as independent of the H_2O stretching motion owing to the separability of the radial and angular wavefunctions of the ground and electronically excited states and hence could be applied to other stretches as well. Previously, good agreement with the FC model was obtained for the photolysis of water from initial rotational states prepared via excitation of the fundamental antisymmetric vibrational stretch [49] and via excitation of an overtone containing four quanta of O–H stretching [62, 64]. Also, the product state distributions resulting from the about 282 nm photodissociation of water molecules excited to the third and fourth OH stretching overtone showed qualitative agreement with the FC model [65]. In the light of these findings it appears that the final OH rotational distributions depend on the initial rotational motion of the water molecule and not on the initial stretching excitation, justifying the separability of the radial and angular wavefunctions of the ground and electronically excited states in the FC calculations.

Despite the fact that branching ratios and final state distributions obtained in state-to-state experiments provide comprehensive information concerning bond breaking, they do not entirely specify the photodissociation process. This is due to the anisotropy of the process in which the polarization of the electric field ε defines a unique direction, relative to which all vectors describing both the parent molecule and the products can be correlated. Consequently, accomplishing characterization of the photodissociation dynamics requires measurement and analysis of the correlations among the parent transition dipole moment $\boldsymbol{\mu}$, the recoil velocity vector of the photofragment $\mathbf{v}$, and its angular momentum $\mathbf{J}$. In order to find the vectorial properties, polarized 193 nm photodissociation of state specific rotational states of H_2O (1, 0, 0) with detection of both polarized broadband and narrowband LIF of OH was performed [68]. The rotational states of water are designated by the total angular momentum $\mathbf{J}$ and subscripts that indicate the projections of $\mathbf{J}$ on the a-axis, K_a, and on the c-axis, K_c. The 3_{03} state, pure in-plane rotation, and the $3_{21} + 3_{22} + 4_{14}$ state, consisting of a mixture of approximate contributions of in-plane (mainly 4_{14}) and out-of-plane (mainly $3_{21} + 3_{22}$) rotations, were prepared. The preparation of a pure out-of-plane rotation was limited by the weakness or resolvability of relevant transitions [69]. For the photodissociation of the 3_{03} state the maximum attainable $\boldsymbol{\mu}$–$\mathbf{J}$ alignment was observed, $A_0^{(2)} = 0.42 \pm 0.10$ for the highest measured J, with about half of this value for the photodissociation of the mixed rotation. In addition, for photodissociation from the 3_{03} state the $\boldsymbol{\mu}$–$\mathbf{v}$, $\mathbf{v}$–$\mathbf{J}$, and $\boldsymbol{\mu}$–$\mathbf{v}$–$\mathbf{J}$ correlations were close to the expected values for an idealized orientation, where $\boldsymbol{\mu}$ of H_2O is parallel to the angular momentum of the OH photofragment and perpendicular to its velocity. These findings confirmed the promptness and planarity of water photodissociation and demonstrated the instrumentality of highly specific preparation of rotations in determination of directional properties of the photodissociation.

3.3. *C_2H_2 and C_2HD*

Acetylene, as one of the most important hydrocarbon molecules, plays a particular role in molecular photophysics and was the subject of numerous theor-

etical and experimental explorations. Despite the extensive attention it received, its photophysical and photochemical properties are still poorly understood, prompting additional studies in view of its unique characteristics. Previous studies focused on the excited vibrational states of the $\tilde{\mathbf{X}}\ ^1\Sigma_g^+$ ground electronic state due to their simplicity and since they represent features relevant to vibrational dynamics in larger systems [14, 70–82]. This state possesses a vibrational density of states growing relatively slowly with energy, leading to fully resolved spectra up to chemically interesting levels of vibrational excitation, $E_{vib} \leq 20\,000\,cm^{-1}$, which is well above the barrier to a bond-breaking isomerization between acetylene and vinylidene [14]. In addition, the stretching and bending frequencies of the C-H oscillators occur approximately with a 5:1 ratio, leading to a weaker coupling to the rest of the molecule than in other molecules where this ratio is about 2:1. Besides, its isotopomer, the monodeuterated acetylene, C_2HD, is particularly interesting since it represents an almost unperturbed energy pattern of vibrational levels [74, 76]. This accidental specificity in C_2HD arises since pairs of levels involving C-H and C-D stretches lie energetically rather far apart, and therefore the effect of the couplings might be reduced. The spectroscopy of the excited electronic states of acetylene [83–85] and its dissociation mechanism [86–93] also gained much interest. These studies indicated that its ground state is linear, while the first two excited singlet states ($\tilde{\mathbf{A}}\ ^1A_u$ and $\tilde{\mathbf{B}}\ ^1A_u$) have planar *trans*-bent configurations. The $\tilde{\mathbf{A}}$–$\tilde{\mathbf{X}}$ and $\tilde{\mathbf{B}}$–$\tilde{\mathbf{X}}$, partially overlapping, absorption systems exhibit long vibrational progressions in ν_3' (the excited state *trans*-bending mode) in the 190–240 and 155–200 nm wavelength regions, respectively. In addition, it was found that both states correlate adiabatically with excited C_2H and ground state H ($C_2H\ (\tilde{\mathbf{A}}\ ^2\Pi) + H(^2S)$) [86, 93]. However, the adiabatic surface has a barrier which inhibits $C_2H\ (\tilde{\mathbf{A}}\ ^2\Pi)$ production and consequently enables predissociation to the ground state products $C_2H\ (\tilde{\mathbf{X}}\ ^2\Sigma^+) + H\ (^2S)$. The latter process is non-adiabatic and may evolve via intersystem crossing to near resonant triplet states and/or internal conversion to high lying vibrational levels of the ground state. The general belief is that intersystem crossing represents the dominant coupling out of the $\tilde{\mathbf{A}}$ state in the near threshold energy range [87–90, 93].

Consideration of the above-mentioned characteristics suggests that disposal of vibrational excitation in specific modes of C_2H_2 or C_2HD might provide different starting points for photodissociation than the photodissociation of vibrationless reactants does. This can reveal entirely different aspects of the state-to-state dynamics and shed new light on this interesting molecular system. Furthermore, the possibility of obtaining isotopic selectivity in the photofragmentation of C_2HD may provide information concerning the nature of the prepared vibrational states and the exit channel interactions governing the bond breaking on the initially excited bound state. To gain some insight on the above raised points, rovibrationally excited C_2HD (in the 15 637–15 735 and 15 256–15 337 cm^{-1} regions) and C_2H_2 (in the 15 480–15 723 cm^{-1} region) were promoted by about 243.1 nm photons to the excited electronic *trans*-bent states $\tilde{\mathbf{A}}\ ^1A_u/\tilde{\mathbf{B}}\ ^1B_u$ and photodissociated. These photons also interrogated the H/D fragments via (2 + 1) REMPI, enabling generation of action spectra, H Doppler profiles and TOFMS.

A representative action spectrum of C_2H_2 (1410^02^0), (2030^00^0) and (2031^10^0) is displayed in the lower trace of figure 4. The vibrational states were designated [75] in the form ($V_1V_2V_3V_4^{l_4}V_5^{l_5}$) with quantum number V_i corresponding to the jth normal mode ν_j: ν_1 and ν_3 are identified as σ_g^+ and σ_g^- C-H stretching modes and ν_4 and ν_5

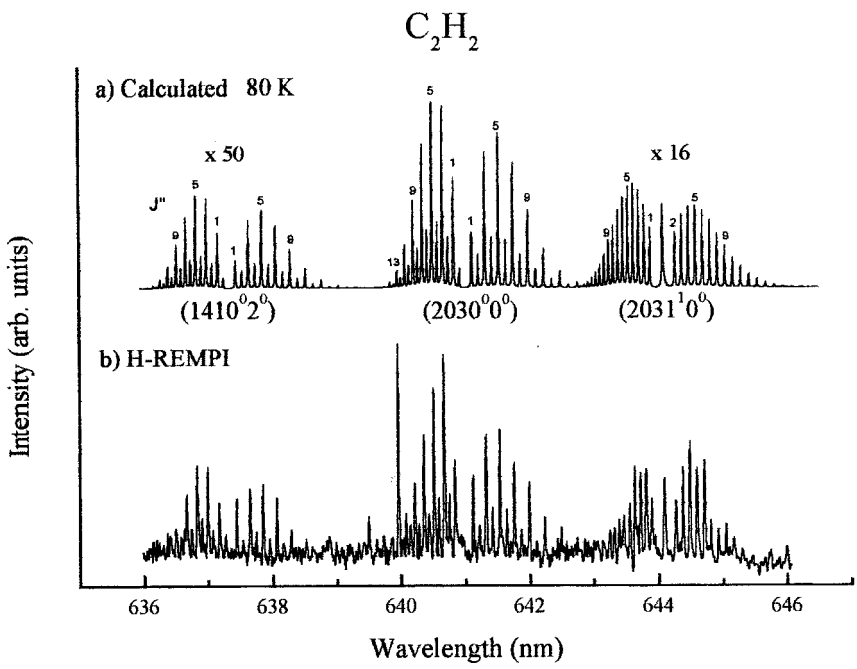

Figure 4. Vibrational overtone excitation spectra of the C_2H_2 (1410^02^0)–(0000^00^0), (2030^00^0)–(0000^00^0) and (2031^10^0)–(0001^10^0) transitions. The simulated absorption spectrum was calculated using rovibrational parameters from [69, 74], nuclear spin degeneracies and Boltzmann distribution at a rotational temperature of 80 K (upper trace). The action spectrum presents the (2 + 1) REMPI intensities of the H photofragments owing to 243.135 nm photolysis (lower trace). ×50 and ×16 are the factors used to scale up the simulated absorption intensities of the (1410^02^0) and (2031^10^0) bands relative to that of (2030^00^0), respectively. The numbers above the peaks in the simulated spectrum assign the rotational levels of the vibrational ground state C_2H_2. Reprinted with permission from Schmid *et al.*, *J. chem. Phys.*, **109**, 8959, © 1998 American Institute of Physics and Schmid *et al.*, *J. chem. Phys.*, **107**, 385, © 1997 American Institute of Physics.

as the π_g (*cis*) and π_u (*trans*) bending modes respectively, while ν_2 is the C-C symmetric stretch (σ_g^+). Superscripts l_4 and l_5 represent vibrational angular momentum quantum numbers. For acetylene, the observed vibrational pattern could be well fitted by employing the NM model [75] or the LM model [71–73]. The (2030^00^0) state comprises excitation of five quanta of C-H stretch, while the combination bands include not only C-H stretch or C-H plus C≡C stretch excitation but also bending. The spectra of the (1410^02^0) and (2030^00^0) bands are characterized by $\Sigma_u^+ - \Sigma_g^+$ transitions including P- and R-branches with intensity alternation of 3:1 ($J'' = \text{odd} : J'' = \text{even}$) owing to nuclear spin statistics. The spectrum of the (2031^10^0) band is typical of a Π_u–Π_g transition and consists of an unresolved Q-branch in addition to the P- and R-branches. The upper trace of figure 4 shows a simulated vibrational spectrum, based on the rotational constants [72, 77], the nuclear spin degeneracies and the Boltzmann distribution at a rotational temperature of 80 K. The C_2H_2 rotational temperature was estimated from the characteristic rotational contour obtained in the action spectrum. Owing to the presence of the hot band transition [(2031^10^0)–(0001^10^0)] in the action spectrum, it

was assumed that the vibrational temperature was higher than the rotational and that no vibrational relaxation occurred, that is $T_{vib} = 300\,K$.

As can obviously be seen, the intensities of the combination bands are far more prominent in the action than in the simulated spectra. The measured integrated intensity of the (2030^00^0)–(0000^00^0) transition is only two times stronger than that of (1410^02^0)–(0000^00^0) and even less for the other band. This contrasts the behaviour encountered in absorption spectroscopy, where only the C–H stretch overtone transition was observed (due to poor sensitivity) [94], or was much more intense than the combination bands [72, 77]. These observations manifest the difference between vibrational absorption and action spectra. Relying on the absorption spectra [77], it was estimated that the $[(2031^10^0)$–$(0001^10^0)]$:$[(2030^00^0)$–$(0000^00^0)]$ intensity ratio was given by the $[(0001^10^0)$:$(0000^00^0)]$ population ratio, for example, about 4.5% at 300 K. The absorption intensity of the $[(1410^02^0)$–$(0000^00^0)]$ relative to $[(2030^00^0)$–$(0000^00^0)]$ was even lower and roughly estimated as about 1%.

The dramatic difference in intensity ratios between the bands in the absorption and action spectra demonstrates their character. The absorption spectra depend on the transition probability for the vibrational transition, $|\langle n|\mu_v|g\rangle|^2$, where $\langle n|$ and $|g\rangle$ are the prepared intermediate and ground vibrational states respectively and μ_v is the vibrational transition dipole moment operator. The action spectra depend, in addition, on the transition probability for photodissociation out of the prepared intermediate state, $|\langle n'|\langle e'|\mu_e|e\rangle|n\rangle|^2$, where $|e\rangle$ and $\langle e'|$ are ground and excited electronic states respectively, μ_e is the electronic dipole moment operator and $\langle n'|$ is the vibrational state in the upper electronic state. Using the Condon approximation to separate out the electronic transition dipole moment matrix element, the overall signal intensity in the action spectra is given by [81]

$$S_n\alpha|\langle e'|\mu_e|e\rangle|^2|\langle n'|n\rangle|^2|\langle n|\mu_v|g\rangle|^2. \tag{2}$$

Hence the signal depends on the electronic transition dipole moment, the FC overlap between the vibrational wavefunctions in both electronic states, $|\langle n'|n\rangle|^2$, and the vibrational excitation probability which, in fact, is directly probed in the absorption experiment. As mentioned above, the intermediate vibrational states, $|n\rangle$, are a linear combination of the zero-order states $|s\rangle$ and $\{|l\rangle\}$ (see equation (1)) and the transition probability in the vibrational overtone excitation step depends on the coefficient of the ZOBS. Thus, in the rovibrational absorption spectra the band intensities depend on the transition strength to the prepared vibrational state, while in the action spectra they depend, in addition, on the transition probability from the prepared state to the electronically excited states and possibly on the channels for photodissociation. Therefore, the enhanced action spectra of the (1410^02^0) and (2031^10^0) bands, which include bends, are related to a preferred transition probability from the prepared state to the upper bent electronic states, $\tilde{\mathbf{B}}\ ^1B_u$ or the $\tilde{\mathbf{A}}\ ^1A_u$. From the above-mentioned experimental results, the roughly estimated enhancement factors are 50 and 16 for excitation from the (1410^02^0) and (2031^10^0) states, relative to that from the (2030^00^0) state, to the upper electronic states. Hence, energizing combination bands that include bending and particularly the *cis*-bend resulted in vibrational wavefunctions on the ground state that improve the overlap with the dissociative wavefunction and drive the photodissociation more effectively than from a state containing mainly C–H stretch. This is supported by the *ab initio* calculation [93] that indicates the occurrence of adiabatic isomerization, between the

trans (more stable) structure and *cis* isomer, from which the photodissociation takes place. Thus, bending excitation of the C≡C-H moiety contributes to the enhancing of the FC factor for the $\tilde{B}\ ^1B_u/\tilde{A}\ ^1A_u \leftarrow \tilde{X}\ ^1\Sigma_g^+$ excitation that dissociates the molecule.

An additional feature, noticed from the comparison of the action spectra to the simulated spectra, is that the positions of the rotational lines in both spectra were preserved, while the intensities were not. Most of the rotational transitions to the (1410^02^0) and (2030^00^0) states follow the intensities of the rotational contours depicted in the simulated spectra (figure 4) representing a regular behaviour, but the R(13) and R(23) transitions to the (2030^00^0) state and several transitions to the (2031^10^0) state are more prominent than in the simulated spectra. Moreover, when the action spectra were monitored at a higher rotational temperature, that is 180 K [94], the intensities of the above-mentioned rotational transitions as well as that of P(25) of the (2030^00^0) band were greatly enhanced. This behaviour points to two kinds of irregularities: in the first irregularity, both R(23) and its counterpart P(25), terminating at the same upper level ($J' = 24$), were enhanced; in the second irregularity only R(13), and not its P(15) counterpart that terminates at the same upper level ($J' = 14$), shows anomalous high intensity. In addition, it was noticed [94] that the yield of the H atom in photodissociation via both R(13) and R(3) (a regular transition) shows a linear intensity dependence on the VIS excitation energy, but with a slope of two for the former and one for the latter. The results indicate single photon absorption in the VIS stage, but higher overall absorption cross-section for R(13) than for regular transitions. Moreover, the R(13) transition also represents a broader Doppler profile and a different fragmentation pattern in the TOF spectrum with a more pronounced C_2^+ signal than for regular transitions [94].

The photodissociation of the different bands, that mainly exhibit a regular rotational contour, was concluded to occur through the $C_2H\ (\tilde{A}\ ^2\Pi) + H$ or vibrationally excited $C_2H\ (\tilde{X}\ ^2\Sigma^+) + H$ channels. As for the irregular rotations, two different types of accidental double coincidence resonances, capable of enhancing the two types of anomalously intense lines, were ascribed. The suggested mechanism for the transitions that show anomalous intensity and share the same upper J' [R(23) and P(25)] is that of coupling between specific rotational levels of the upper vibrational state and energetically close lying zero-order states. Presumably, these states are dark zero-order states that carry no oscillator strength from the ground state, but that enhance the signal in the electronic excitation step owing to better FC factors. The involved dark states are assumed to contain bends and C≡C stretches possessing a better FC overlap with the bent upper state. This agrees with the above discussion about the large variation in signal intensity when preparing combination bands versus C-H stretch overtone and also with the observed H Doppler profile and the fragmentation pattern.

For R(13), excitation of an additional weak overlapping transition, by the VIS photon, was proposed. This transition was too weak to be observed in VIS absorption, but showed up strongly via electronic excitation and hence was observed in the action spectra. A possible candidate was the (0509^11^{-1}) state [75, 77]. This state contains nine quanta of *trans*-bend excitation and therefore was expected to increase the FC factor and to lead to higher intensity in the action spectra. Since the excitation of acetylene is in the 15 600 cm^{-1} region to a level containing so many bending quanta, the possibility of mixing in vinylidene (isomer of acetylene) could be also suggested [94]. The VIS absorption was followed probably by two UV photons,

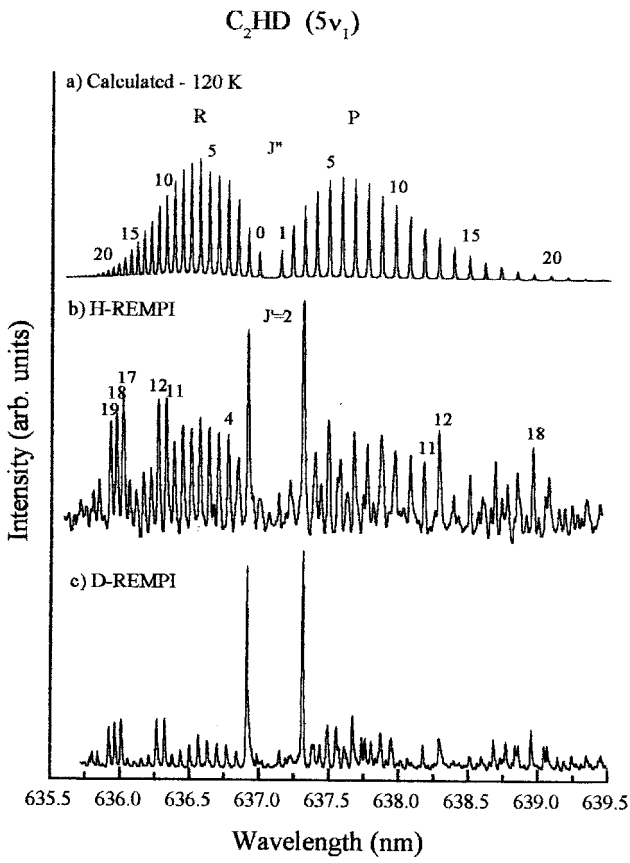

Figure 5. Vibrational overtone excitation spectra of the $5\nu_1$ state of C_2HD: (*a*) simulated absorption spectrum calculated using rovibrational parameters from [69] at a temperature of 120 K. (*b*) and (*c*) The action spectra of H and D photofragments as a result of about 243.1 nm photolysis at 150 and 250 μJ, respectively. The numbers above the peaks in the simulated spectrum label the rotational levels of ground-state C_2HD and those in the action spectrum mark the rotational levels of $5\nu_1$ for which preferential enhancement is observed. (Reprinted from Arusi-Parpar *et al.* [95], with permission from Elsevier Science.)

that could be absorbed through an accidental double coincidence resonance, and differ from that of regular transitions where only one UV photon was absorbed. Owing to the two-UV-photon absorption a sequential elimination of two H atoms or a synchronous C-H bond cleavage was inferred, thus favouring C_2^+ generation. This assumption is supported by the high intensity of the C_2^+ fragment in the TOF spectrum and by the wider H Doppler profile [94].

Like HOD, the VMP of C_2HD again offers two distinct isotopic channels and is a very challenging system [95]. C_2HD was energized, alternatively, with five quanta of C-H ($5\nu_1$), four quanta of C-H and one quantum of C-D ($4\nu_1 + \nu_3$), or three quanta of C-H plus one quantum of C-C, one quantum of C-D and two *cis*-bends ($3\nu_1 + \nu_2 + \nu_3 + 2\nu_5$) prior to its promotion by about 243.1 nm photons to the upper electronic states. Figures 5 and 6 represent action spectra of H and D photofragments ((*b*) and (*c*)) as a function of excitation and the simulated absorption spectrum (*a*) of these bands. The $H + C_2D$ and $D + C_2H$ photofragments were the outcomes

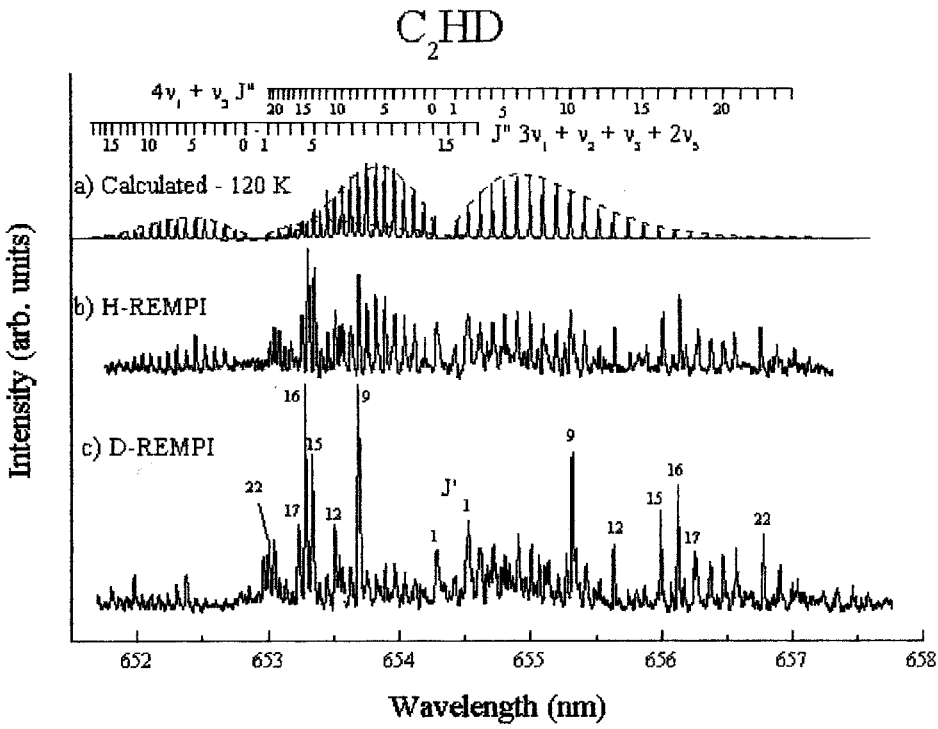

Figure 6. Vibrational overtone excitation spectra of the $4\nu_1 + \nu_3$ and $3\nu_1 + \nu_2 + \nu_3 + 2\nu_5$ states of C_2HD: (*a*) simulated absorption spectrum at 120 K, (*b*) and (*c*) action spectra of H and D photofragments as a result of about 243.1 nm photolysis at 220 μJ. The rulers above the simulated spectrum label the rotational levels of ground-state C_2HD and the numbers in the action spectrum mark the rotational levels of $4\nu_1 + \nu_3$ that are standing out from the rotational contour. (Reprinted from Arusi-Parpar *et al.* [95], with permission from Elsevier Science.)

of C-H and C-D bond cleavage respectively. The simulations were based on known molecular constants of the $5\nu_1$ and $4\nu_1 + \nu_3$ states [76]. The simulations represent spectra of Σ^+–Σ^+ bands including P- and R-branches and that of $5\nu_1$ is similar to the Fourier transform vibrational spectrum [76]. The H and D peaks (5(*b*), 6(*b*) and 5(*c*), 6(*c*)) track the positions of the rotational lines in the simulation (5(*a*), 6(*a*)), and the yield of both H and D photofragments was enhanced upon photolysis with that of H being higher than that of D.

Although the excitation coefficient of the $5\nu_1$ state is less than 10^{-6} of the fundamental C-H stretch [76], a large signal is observed, showing extremely efficient production of H and D. The intensity ratio between $5\nu_1$ and $4\nu_1 + \nu_3$ as measured from the amplitudes of R transitions of regular rotational states ($J' = 6$–8) was 1.5 ± 0.1. This ratio agrees well with that of 1.55, measured from absolute transition dipole moments in direct absorption experiments [76]. The almost comparable intensity ratios in action spectra and in absorption indicate similar character of the two bands that contain only stretches. This is probably due to the fact that in the second step of excitation to the upper electronic states the transitions do not differ much in their FC factors. As for $3\nu_1 + \nu_2 + \nu_3 + 2\nu_5$, no data concerning its intensity in direct absorption are available, and therefore the influence of the FC factor on the action spectrum intensity could not be determined.

Like in C_2H_2, the most intriguing observation is that pairs of rotational transitions terminating in the same upper J' ($J' = 2$, 11, 12, 17–19, 21, 22 of $5\nu_1$ and $J' = 1$, 9, 12, 15–17, 22 of $4\nu_1 + \nu_3$), in both the H and D action spectra, are more pronounced and stick out from the P and R regular rotational contour. It is seen that some of the transitions exhibit an intensity of more than an order of magnitude higher than that for a Boltzmann distribution. In contrast, the absorption spectrum of $5\nu_1$ varies smoothly with J' and follows a Boltzmann distribution [76]. The observation that both P- and R-branch transitions sharing similar J' deviate from the regular behaviour was attributed, as in C_2H_2 (R(23) and P(25)), to couplings with dark zero-order states. A similar behaviour was encountered in the VMP of isocyanic acid, HNCO, excited with three quanta of N-H stretching that was coupled to a state containing N-C-O bending vibration [96]. This excitation prompted strongly the photodissociation, but hindered the bimolecular reaction with Cl atoms.

Moreover, the rovibrational preparation did not effect only the transition intensities in the action spectra, but also the H/D branching ratio. For example, for $5\nu_1$, the H/D branching ratios were 4.9 ± 0.5 for the regular line (e.g. $J' = 4$) and 1.5 ± 0.2 for the irregular (e.g. $J' = 2$) [95]. For $4\nu_1 + \nu_3$, the H/D ratio for regular lines was in the range of 2.5–3.8, while for irregular transitions it was 0.9–1.5.

The results for the regular lines demonstrate that there is a change in the yield and in the H/D branching ratio following bond fission in C_2HD ($5\nu_1$) and C_2HD ($4\nu_1 + \nu_3$), also as a result of preparation of different vibrational states. The combined energy (VIS + UV) decreases only slightly from about 7.05 eV for $5\nu_1$ to about 7.0 eV for $4\nu_1 + \nu_3$ and therefore it is unlikely to be the reason for the difference in branching ratio. A possible explanation is that in $5\nu_1$ only the C-H bond is extended, while in the $4\nu_1 + \nu_3$ state the C-D bond is extended as well. In both cases the C-H bond is cleaved preferentially, but the H/D ratio of 4.9 for regular lines in $5\nu_1$ is reduced to 2.5–3.8 in $4\nu_1 + \nu_3$. The effect is even more dramatic when irregular rotational states are prepared prior to photodissociation since then the preference is reduced to almost statistical H/D ratios (0.9–1.5). This is, most probably, a result of the coupling of the prepared J' with zero-order dark states. Possible candidates for interaction are states that include combinations of C-D stretches and bends or C≡C stretches and bends. This interaction leads to extension of the C-D bond and to enhancement of its cleavage as a result of better FC overlap, which is represented by the higher intensities in the action spectra and, moreover, by the different H/D branching ratios. This is also supported by noting the experimental conditions in our study, where H and D action spectra were monitored at two different photodissociation wavelengths (243.135 and 243.069 nm respectively, about 11 cm^{-1} apart). Nevertheless, identical transitions sharing similar values of J were more pronounced in the action spectra of both H and D, pointing to the effect of the resonances of J with other states that are then more effective in excitation to the upper electronic state. In summary, the rotational specific VMP of C_2HD serves as a fascinating example of product identity and H/D branching ratio control not only via excitation of different skeletal motions, but even by preparation of neighbouring rotational states. The action spectra observed in the VMP of C_2H_2 and C_2HD show that the composition of the rovibrational state strongly affects the photodissociation dynamics and thus calls for a study of even more complex systems. Indeed, in what follows the efforts directed toward the study of VMP of larger molecules are described.

3.4. *Propyne-d_3*

Propyne ($CH_3C{\equiv}CH$), an acetylene homologue, is an excellent molecular system for testing the effect of initial vibrational excitation on photodissociation outcome. Its unique features include availability of two C-H oscillator types, a methyl group that does not internally rotate and an acetylenic C-H oscillator that is slightly higher in frequency than the other C-H stretches and is thereby somewhat decoupled from them. Like in acetylene, the stretching and bending frequencies of the acetylenic C-H stretch are of a ratio of about 5:1, leading to its weaker coupling to the rest of the molecule. In addition, propyne is characterized by resolved and mostly unperturbed rotational structures, up to high excitation energies of the acetylenic C-H stretch [97] and therefore was extensively studied to investigate IVR [97–101]. These studies explored the effect of different C-H type stretches, where the energy is initially localized in specific bond types, on IVR rates, couplings and possible pathways. Also, the vibrationless ground state photodissociation of propyne and its isotopomers at 193 nm revealed that only the C-H(D) acetylenic bond is cleaved [102–105], although its strength is significantly larger than that of the C-H(D) methyl bond [106–109]. We decided to check if product identity might be affected as a consequence of vibrational pre-excitation as compared to the nearly isoenergetic 193 nm photodissociation of vibrationless ground state propyne and selected propyne-d_3, $CD_3C{\equiv}CH$, as a test model. Therefore, $CD_3C{\equiv}CH$ was excited in the region of three quanta of C-H acetylenic stretch ($3\nu_1$) and photolysed by about 243.1 nm photons [107].

The top trace of figure 7 shows the PA (absorption) spectrum while the two bottom traces the jet-cooled action spectra of D and H respectively for $3\nu_1$ pre-excited propyne-d_3. Comparison of the action spectra to the PA spectrum clearly shows that the two Q-branches, corresponding to the $3\nu_1 + \nu_{10} - \nu_{10}$ and $3\nu_1 + 2\nu_{10} - 2\nu_{10}$ hot bands (ν_{10} is the degenerate C-C≡C bend with a fundamental frequency as low as 306.4 cm^{-1}), were absent in the action. Also, the contours of the P- and R-branches in the action spectra are considerably contracted with maxima at lower values of J relative to those observed in the PA spectrum, showing the efficacy of the rotational cooling. However, most important is the extremely efficient D and H photofragment production upon rovibrational excitation and photolysis of $CD_3C{\equiv}CH$ ($3\nu_1$). Owing to its structure, it is obvious that the released H atom photofragments came from the acetylenic C-H and the D photofragments from the methyl C-D. The D yield dominated and the D/H ratio equalled 2.5 ± 0.2, approximately reflecting the stochiometric ratio. It is striking that although the combined energy for photodissociation, 50 827.4 (50 838.6) cm^{-1} for H(D), was close to that in 193 nm photolysis, 51 813 cm^{-1}, the photodissociation outcome was completely different. The small energy mismatch, between the two does not seem to be the origin for the altered outcome.

The cleavage of the acetylenic C-H in the photodissociation of vibrationless ground state was attributed to its proximity to the C≡C bond, along with initial excitation via a $\pi^* \leftarrow \pi$ transition [105] and H atom production on the excited state. Theoretical calculations on propyne [106] suggested that the apparent preference for H atom elimination with a bond strength of 130.5 kcal mol^{-1} (5.66 eV) over the one with an energy of 88.7 kcal mol^{-1} (3.85 eV) could be rationalized in terms of the structure of the excited $S_2(cis)$, $2\ ^1A'$ state, where the C-H bond is lengthened and weakened and no barriers for H atom elimination exist.

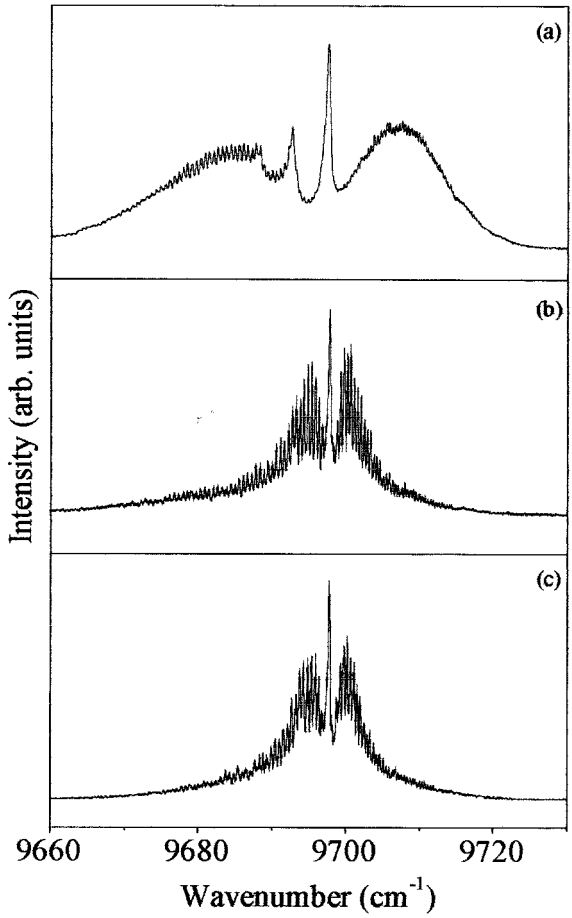

Figure 7. Vibrational overtone excitation spectra of the $3\nu_1$ C—H acetylenic stretch region of $CD_3C{\equiv}CH$. (*a*) Photoacoustic absorption spectrum in a static cell at a pressure of 30 Torr and room temperature, (*b*) D and (*c*) H action spectra obtained from about 243.1 nm photodissociation of jet-cooled molecules using about 2.5% $CD_3C{\equiv}CH$ seeded in Ar at a backing pressure of about 760 Torr. The intensity scale of each panel is different. Reprinted with permission from Chen *et al.*, *J. chem. Phys.*, **113**, 5134, © 2000 American Institute of Physics.

In the VMP process (combined energy of about 6.30 eV) the excitation was presumably also to the S_2, $2\,{}^1A'$ state that is overlapped by the S_1, ${}^1A''$ [106] state. These states are characterized by bent geometry, facilitating absorption from the initially vibrationally excited $CD_3C{\equiv}CH$. In fact, the preparation of the vibrational state the C-H acetylenic bond results in its elongation, however, on the time-scale of our experiment, the energy decays from it to other modes distorting its geometry. Therefore, the efficient production of H and D could be a result of the improved FC overlap between the vibrationally excited molecule and the dissociative wavefunction. Resemblance can be found in what was mentioned above for the about 243.1 nm photodissociation of vibrationally excited acetylene prepared in the (1410^02^0) state where a high photodissociation efficacy was observed due to its preferred connection with the upper PES of *cis* structure.

Since the upper PESs involved in the VMP of $CD_3C{\equiv}CH$ ($3\nu_1$) are similar to those in the photodissociation of vibrationless ground state molecules, it is likely that the acetylenic H loss occurs adiabatically on these PESs. On the other hand, for methyl D, it was implied that internal conversion to the ground state occurred, based on evidence from experiments that tracked the energy content of the H and D photofragment, that is the Doppler profiles. The H profile was broader than that of D, but the calculated average translational energies of the two were almost identical (0.48 ± 0.02 eV for H and 0.49 ± 0.03 eV for D). This means that completely different average fractions of the available energy were released as translation $\langle f_T \rangle$, 0.75 for the H channel and 0.20 for D. For acetylenic bond breaking, the H photofragment was released with relatively large average translational energy content, indicating rupture on the excited PESs, while for methyl, the D had a much lower energy content, due to dissociation from a hot ground state where the process is more likely to be statistical.

To conclude, the fact that in direct photodissociation only the acetylenic bond was broken, while in VMP the methyl bond was cleaved as well, is due to sampling of different portions of the upper PESs by the vibrationally excited wavefunction. In these regions, internal conversion to the ground state and a redistribution of the energy between vibrational degrees of freedom of the propargyl radical ($CD_2C{\equiv}CH$) might be more efficient and therefore reject methyl D atoms with low translational energy. Thus, the about 243.1 nm photodissociation of $CD_3C{\equiv}CH$ ($3\nu_1$) diminishes bond selectivity observed in the 193 nm direct photodissociation and emphasizes the impact of initial state preparation on the photodissociation dynamics.

3.5. *Hydrochlorofluorocarbons*

Exploration of molecular transformations occurring in photodissociation of vibrationally excited HCFC methane and ethane derivatives provides an opportunity for testing the effect of initial vibrational excitation on product branching and identifying the spectral features as well as estimates for the time-scales for intramolecular energy transfer. The photochemistry of HCFCs was first studied in the gas phase at relatively high pressures, in the absence or presence of different added gases [108, 109]. Recently, their photochemistry raised considerable interest due to their introduction as interim replacements to the ozone destroying chlorofluorocarbon (CFC) compounds [110–113]. These studies established that the HCFCs release mainly Cl atoms and to some extent H atoms during their photofragmentation in the first absorption band [111, 112]. The loss of open shell electronic states of Cl atoms is of importance not only because of the atmospheric relevance, but also for dynamic studies. In particular, studies that determine the spin–orbit branching ratios [114–119] and the $\boldsymbol{\mu}$–$\mathbf{v}$ correlation are measures of the involved PESs and the adiabatic and non-adiabatic interplay during photodissociation. The general outlines of the experiment on HCFCs were similar to that on acetylene and propyne-d_3. The about 235/243 nm photons photodissociated pre-excited $N = 3$, 7/2, 4 and 5 C-H stretch–bend polyad components (see below) of $CHFCl_2$ [120], and the fundamental symmetric methyl stretch (ν_2) and the second ($3\nu_{CH}$) and third ($4\nu_{CH}$) methyl overtones of CH_3CFCl_2 [121]. Room temperature PA and jet-cooled action spectra of Cl, Cl* and H photofragments were monitored. The action spectra revealed details of the vibrational dynamics occurring subsequent to the excitation of the isolated C-H stretch of $CHFCl_2$ and the C-H methyl stretch

of CH_3CFCl_2. The description starts with the methane derivative and continues to the ethane derivative of HCFC.

A portion of a representative room temperature PA spectrum along with the jet-cooled action spectra in the region of the $N = 7/2$ polyad of $CHFCl_2$ is shown in figure 8. The PA spectrum was assigned by a model involving coupling between the CH stretching and the CH bending motions [122]. The vibrational overtone bands were labelled as N_j components, where an integral N represents a polyad quantum number consisting of N CH stretch quanta in the ZOBS, and a half-integral N contains N CH stretch quanta combined with the higher ($\nu_2 = 1317.2\,cm^{-1}$) or lower ($\nu_7 = 1242.6\,cm^{-1}$) frequency bending. The Hamiltonian matrix is therefore block diagonal in N, where each block contains one C–H polyad with a certain value of $N = v_S + v_1 + v_2$ (v_S is the quantum number of the pure stretching basis states, v_1 is the quantum number for one of the bendings and v_2 for the other). This model accounts for the anharmonic coupling of the CH stretch ($\nu_1 = 3024.8\,cm^{-1}$) with either of the two CH bends via a 1:2 Fermi resonance, and for the coupling of the two bends by a Darling–Dennison resonance. This is via adjacent off-diagonal elements of the Hamiltonian that account for cubic (Fermi resonance) and quartic (Darling–Dennison) coupling. This interaction produces mixed states, forming the polyad components, which are labelled by a subscript j, starting from the highest frequency to the lowest.

The PA spectrum of the $N = 7/2$ polyad was found to be similar to the Fourier transform infrared (FTIR) spectrum [122]. The portion presented in figure 8(*a*) includes the main features observed for this polyad. Several additional peaks of much lower intensity were observed at lower frequencies and they also correspond to those observed in the FTIR spectrum. The appearance of only two prominent peaks in the $N = 7/2$ polyad and of one peak in the $N = 3$ and 4 is due to the low CH bend frequencies which interact relatively weakly, via the Fermi resonance, with the CH stretch.

The bands observed in the PA spectra are of different types and they represent the contributions resulting from the three dominant isotopomers $[CHF^{35}Cl_2]$: $[CHF^{35}Cl^{37}Cl]$:$[CHF^{37}Cl_2] \cong 9:6:1$ according to the occurrence of the two stable Cl isotopes. These bands are related approximately to CH stretch overtones and to their combinations with bends and therefore possess different shapes, depending on the character of the involved vibrations. The $CHFCl_2$ is an asymmetric top belonging to the C_s point group for identical chlorine atoms and reduces to C_1 for different chlorine isotopes. In C_s, the v_1 CH stretch and the v_2 CH bend are of a′ and the v_7 CH bend of a″ symmetry, while in C_1 the CH stretch and bends are of type a [123, 124]. Owing to their symmetry, the observed bands are characterized by different shapes, where the 3_1 and 4_1 components demonstrate C type prevalancy, the $7/2_1$ B type and the $7/2_2$, which is a combination of the stretch with the bend of a″ is of A type (see figure 8).

The observed PA spectra represent not only contributions from the dominant isotopomers of $CHFCl_2$ but also contain transitions that are related to the hot bands observed in the fundamental region. The $CHFCl_2$ comprises several fundamentals of low frequency, less than $1000\,cm^{-1}$, the lowest being the ClCCl bending, v_6 (a′) at $277.2\,cm^{-1}$. Therefore, about 37% of the population are in these low vibrations at room temperature (compared with the zero point level population of 63%). It is expected that transitions from these states will appear in the proximity of the C–H

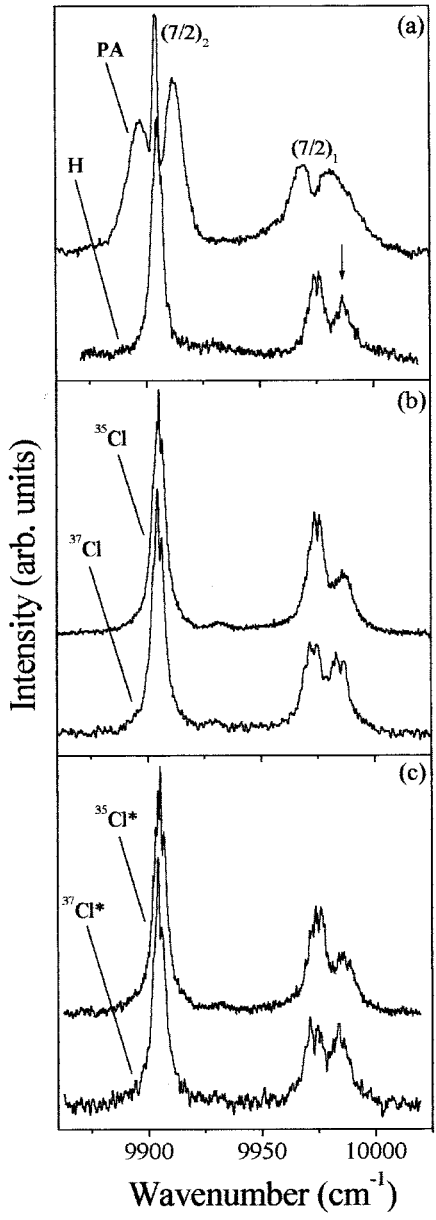

Figure 8. Vibrational overtone excitation spectra of the dominant features of the $N = 7/2$ polyad of $CHFCl_2$: (*a*) photoacoustic absorption spectrum and H action spectrum, (*b*) ^{35}Cl and ^{37}Cl action spectra and (*c*) $^{35}Cl^*$ and $^{37}Cl^*$ action spectra. The arrow designates the $7/2_3 + \nu_6$ combination band observed only in the action spectra due to congestion elimination. The intensity scale is different for each trace. Reprinted with permission from Chen *et al.*, *J. chem. Phys.*, **114**, 9033, © 2001 American Institute of Physics.

polyad components but at lower frequency (often due to negative values of the anharmonicity constants).

Comparison of the PA spectrum with the action spectra of the H, ^{35}Cl, ^{37}Cl, $^{35}Cl^*$ and $^{37}Cl^*$ photofragments (figure 8, lower trace of (*a*), and (*b*) and (*c*)) of the

$7/2_1$, $7/2_2$ polyad components show the extensive contraction that occurs in the latter owing to the rotational cooling. Similar behaviour was observed for the 3_1 and 4_1 polyad components. This narrowing and the merging of the P- and R-branches with the Q-branch result in almost undistinguishable PQR envelopes in the A and C bands and in a much narrower B band. The polyad components in the jet-cooled action spectra exhibit overall contours in the range 19–25 cm^{-1} in comparison with 45–60 cm^{-1} for the room temperature spectra. This clearly indicates that most of the spectral widths in the room temperature spectra arise from rotational inhomogeneous broadening.

An important advantage provided by action spectra is the congestion reduction, which allows in favourable cases observation of new features that are otherwise overlaid by other bands. An example of a new feature that was not observed in the PA spectrum is shown in the action spectra of the $7/2_1$ region. The separation between the $7/2_1$ component and the new feature, indicated by the arrow (figure 8), is $13 \pm 1\,cm^{-1}$ and the ratio of their integrated intensities is 0.7 to 0.3. Employing a simple two-level model [13] to describe resonance and using the observed energies of the perturbed bands and the relative intensities, the unperturbed energies (the diagonal elements) which are coupled by the off-diagonal coupling constant W can be determined. Using energies of 9988 and 9975 cm^{-1} for the perturbed bands of the $CHFCl_2$ isotopomer and their relative intensities of 0.3 and 0.7 respectively, enables derivation of the zero-order energies 9984 and 9979 cm^{-1} and $|W| = 6\,cm^{-1}$.

Low-order resonances involving the change of three or four vibrational quanta and coupled via third- and fourth-order anharmonic terms in the vibrational Hamiltonian are of importance in controlling vibrational energy redistribution and therefore might be involved here as well. Compilation of an energy level diagram of possible perturbing states of a′ symmetry that could be coupled via cubic or quartic terms to the $7/2_1$ state of similar symmetry revealed the possible states within $\pm 100\,cm^{-1}$ [120]. From the compiled states we could see that almost all states are quite separated from the $7/2_1$ state, except the $7/2_3 + v_6$ state which involves a higher polyad component, $7/2_3$, and the v_6 ClCCl bend. Therefore, it is likely that this is the only state that could be coupled by the above-mentioned W of about 6 cm^{-1}. The energy of the $7/2_3 + v_6$ state that amounts to 9988 cm^{-1} is in close agreement with the zero-order energy of 9983.8 cm^{-1} of the feature mentioned above, and the small energy mismatch should not be prohibitive when the anharmonicities are included. The combination of the $7/2_3$ component with the ClCCl mode seems very likely since they are very close in energy, as demanded by the deperturbation.

The splitting between the $7/2_1$ component and the nearly resonant state indicates that the period of the vibrational oscillation is of $1/c\Delta v$, or about 3 ps, and the redistribution time to the ClCCl bend is about 1.5 ps. This is 30 times longer than the time for redistribution between stretch and bend, that is, 50 fs, which was deduced in the computation of the time evolution from the effective Hamiltonian [120, 122]. The longer time is a measure of the time-scale for energy flow between the $7/2_1$ and $7/2_3 + v_6$ zero-order states, when the former is prepared. A similar behaviour was observed in other molecules with isolated C–H stretches, such as $CHCl_3$ [125] and CHF_3 [126]. For example, in $CHCl_3$ the energy redistribution for the 4_1 state to the CCl_3 'umbrella' vibration is almost a factor of 100 slower than the about 50 fs redistribution time between stretch and bend.

The action spectrum displayed in figure 8 does not only provide a wealth of dynamical information concerning the prepared vibrational states, but also exhibits and emphasizes the significant increase in Cl, Cl* and H photoproducts yield as a result of VMP, relative to the background one photon photodissociation. Hence, by measuring the yields of the different photofragments and particularly the branching ratios between them, some information concerning the dynamics on the upper PESs can be revealed. Comparison of the total Cl yield, in both spin–orbit states, with that of H showed that the former was enhanced four times more than the latter for the VMP of the 3_1, $7/2_2$ and 4_1 components [120]. This finding emphasizes that although the C-H stretch was initially extended, the cleavage of the C-Cl bond was more efficient. This agrees with the above analysis that showed that the vibrational energy redistribution occurs on a time-scale of picoseconds. Consequently, for the laser pulse widths employed in our experiment it is obvious that mixed states were prepared and the energy was already redistributed into the modes corresponding to the heavy atoms during the excitation step. Extension of the C-Cl bond, which becomes the reaction coordinate, may lead to favourable FC factors with the upper PESs, probably due to the absorption characteristics related to a σ^*_{C-Cl} n transition [127, 128].

By accounting for the transition probability ratios of the tagged fragments [30, 31, 119] the REMPI signals were converted into Cl*/Cl and H/[Cl + Cl*] branching ratios. The branching ratios for Cl*/Cl in VMP of $CHFCl_2$ are close to 0.5 independent of the prepared polyad component. The H/[Cl + Cl*] is in the range 0.11–0.15, pointing again to the low fraction of produced H relative to that of Cl and Cl*.

In addition, the experimental ^{35}Cl and $^{35}Cl^*$ ion arrival time profiles following the about 235 nm photodissociation of $CHFCl_2$ prepared in the Q-branch (comprising several unresolved rotational states) of the 3_1, 4_1 and 5_1 vibrational states were measured and are displayed in figure 9. These profiles represent the VMP 'net' profiles, obtained by removing the contribution, when significant, resulting from the about 235 nm photodissociation of vibrationless ground state molecules (vibrational excitation laser off) from the signal monitored when both the vibrational excitation laser and the UV laser were on [120]. The observed profiles were obtained with the polarization of the photolysis/probe UV laser parallel or perpendicular to the TOFMS axis and with the polarization of the IR/VIS vibrational excitation laser axis remaining fixed with perpendicular polarization. The profiles of both Cl and Cl*, taken under these polarization conditions, are shown in figures 9(*a*)–(*c*). No influence on the polarization of the VIS/IR laser was observed and the profiles showed a similar shape even when the polarization was parallel to the TOFMS axis. This indicates that the vibrational excitation to the Q-branch of the 3_1, 4_1 and 5_1 states does not induce significant alignment to the molecules.

The Cl and Cl* photofragment spectra, shown in figures 9(*a*) and (*b*), indicate that the profiles are doubly peaked for the parallel polarization of the UV laser and singly peaked for the perpendicular polarization. The double peaks are caused by the formation of Cl and Cl* photofragments of equal translational energies but with velocity vectors pointing toward and opposite to the flight axis. The shape of the profiles indicates that both Cl and Cl* photofragments are released predominantly through a parallel electronic transition with a positive β [30–34]. Also, from comparison of the profiles of Cl and Cl* obtained in VMP via the intermediate state 5_1 with those via 3_1 and 4_1 it is evident that the intensities of the centres of the

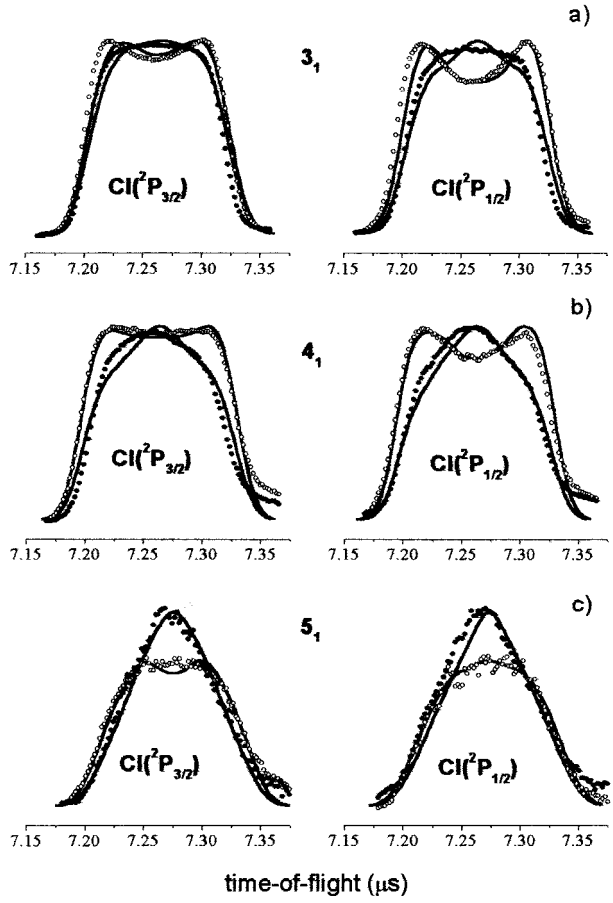

Figure 9. Arrival time distributions of Cl ($^2P_{3/2}$) and Cl ($^2P_{1/2}$) photofragments produced in the about 235 nm photolysis of $CHFCl_2$ pre-excited to the Q-branch of the (*a*) 3_1, (*b*) 4_1 and (*c*) 5_1 states. Open circles and solid points are the experimental data points taken with the polarization of the UV photolysis/probe laser parallel and perpendicular respectively to the TOFMS axis. The polarization of the overtone excitation laser was perpendicular to the TOFMS axis. Solid lines are the simulations of the corresponding profiles. These lines denote the best fit velocity distributions, with constant β, finite time response of the apparatus (modelled as a Gaussian with 20 ns full-width-half-maximum) and Doppler selection by the finite bandwidth of the probe laser (modelled as 0.3 cm^{-1} at the one-photon wave number). Reprinted with permission from Chen *et al.*, *J. chem. Phys.*, **114**, 9033, © 2001 American Institute of Physics.

arrival time profiles increase and are much more pronounced via 5_1. This happens because the profiles are monitored under similar conditions except for the excitation wavelengths employed for the preparation of the 5_1 and 3_1 and 4_1 states. Therefore, the increase in the intensity of the centre of the arrival time distribution is attributed to an increase in production of Cl and Cl* photofragments with nearly zero centre of mass (cm) translational energies. The β parameters and the velocity distributions, $P(v)$, of the Cl and Cl* photofragments, were extracted by simulating the TOF spectral profiles [120]. The distributions of both Cl and Cl* resulting from the VMP of 3_1, 4_1 are significantly narrower than that of the 5_1 state. We also observed that the broadening of the latter, results from production of 'faster' Cl and Cl*

photofragments as well as slower Cl and Cl*. The production of faster Cl and Cl* photofragments arises from higher combined energies (IR/VIS + UV) employed in the VMP of $CHFCl_2$ (5_1) (about 56 459 cm^{-1} (about 7.0 eV)) than in (4_1) (about 53 873 cm^{-1} (about 6.7 eV)) and (3_1) (about 51 236 cm^{-1} (about 6.4 eV)). The combined energies in the VMP of $CHFCl_2$ (3_1), (4_1) and (5_1) exceed that required for the loss of one Cl atom, but the first two do not surpass the threshold for a three-body process where two ground state Cl atoms are released. Therefore, it seems likely that the slower Cl and Cl* photofragments, observed in the VMP of $CHFCl_2$ (5_1), emerge from the three-body decay, either synchronous concerted, where two C-Cl bonds are broken simultaneously, or sequential [129].

The recoil anisotropies also provide some information regarding the mechanism of bond breaking. It was seen that the Cl and Cl* arising from about 235 nm photodissociation of $CHFCl_2$ (3_1), (4_1) and (5_1) via two- or three-body processes possess positive anisotropies, lower than the limiting values. The β parameters of Cl increase somewhat with increasing combined energy, rising from $\beta = 0.14 \pm 0.05$ to 0.27 ± 0.06, and to 0.47 ± 0.07, while those of Cl* are nearly constant with values of $\beta = 0.36 \pm 0.06$, 0.43 ± 0.05 and 0.34 ± 0.04. The magnitude and sign of β are related to the orientation of the transition dipole moment $\boldsymbol{\mu}$ in the parent molecule, the symmetry of the excited state and the excited state lifetime. The theoretical limit for the β parameter, with $\boldsymbol{\mu}$ parallel to the line connecting the two Cl atoms, was calculated and estimated to be about 1.1 (based on a Cl-C-Cl bond angle of 112° in $CHFCl_2$) [110]. In 193 nm photodissociation of vibrationless ground state $CHFCl_2$ molecules, a β of 0.5 ± 0.1 was measured indicating a partial loss of anisotropy [110]. This loss was attributed either to a geometrical rearrangement during dissociation or to a small contribution of an electronic transition of A′ A′ symmetry overlapping the dominant A″ A′ transition.

The β values obtained in the VMP experiment are also positive, presumably due to the access to similar upper electronic states as in the 193 nm photodissociation anticipating that A′ and A″ transitions are also involved in the absorption from the vibrationally excited state. Indeed, calculations [130] have shown that two transitions of A″ and two of A′ symmetry underlie the first absorption band of $CHFCl_2$, related to the σ^* n transition, and that the predominant contribution rises from the lowest energy A″ transition and some from one of the A′. Relying on the accessibility of the upper dissociative states it is conceivable that the dissociation is prompt and it does not seem that the rotational motion accounts for the reduction of β from its limiting value. Thus, the observation of less than limiting β values emerges from dynamical factors. From the measured β it is inferred that both Cl and Cl* are produced as a result of simultaneous absorption to both A″ and A′ states that mix, probably, via curve crossing to release Cl and Cl*. Also, due to the increase in the β value corresponding to Cl, it is likely that the contribution of the A″ state to this channel increases with increasing combined energy.

The observed increase in the Cl channel anisotropy in VMP of $CHFCl_2$ molecules promoted from 5_1 relative to those from 4_1 and 3_1 is a hint for a concerted three-body decay. This is since in the case of sequential three-body decay one would expect a lower β parameter than in the two-body case owing to the increased dissociation lifetime. Relying on the observation of the increase in β it seems likely that the concerted three-body decay is responsible for the slow Cl. As for Cl* photofragments, owing to the small decrease in β in VMP of $CHFCl_2$ (5_1) relative to that in (4_1), it might be that a sequential three-body decay is also involved. These

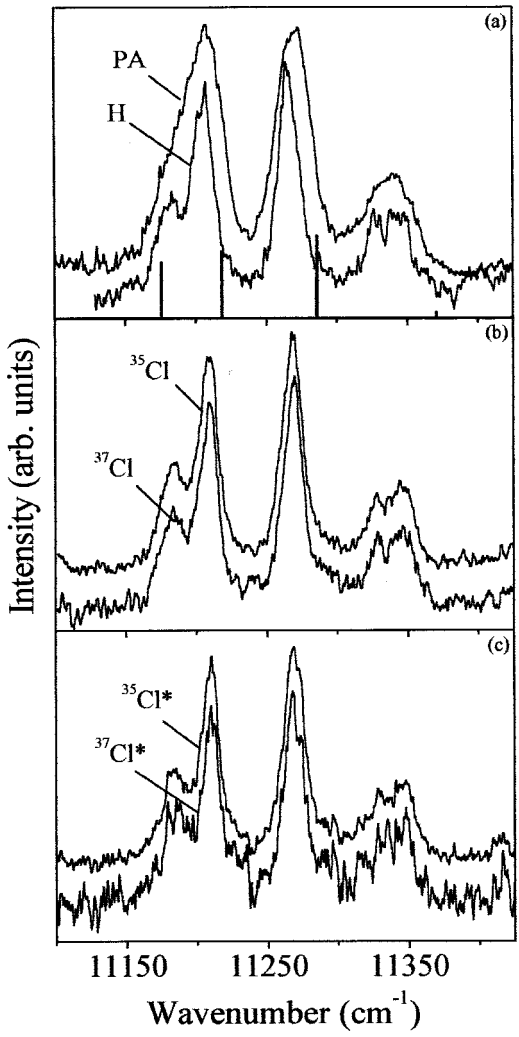

Figure 10. Vibrational overtone excitation spectra of $4\nu_{CH}$ of CH_3CFCl_2: (*a*) PA absorption spectrum at room temperature and H action spectrum, (*b*) ^{35}Cl and ^{35}Cl* action spectra and (*c*) ^{37}Cl and ^{37}Cl* action spectra. The action spectra are of jet-cooled samples. The stick spectrum on the wave number axis of panel (*a*) designates the eigenvalues and eigenvectors' squared coefficients of the zero-order bright state, obtained from the simplified LM model including Fermi resonances. The intensity scale is different for each spectrum. Reprinted with permission from Melchior *et al.*, *J. chem. Phys.*, **112**, 10 787, © 2000 American Institute of Physics.

results suggest that the photodissociation of $CHFCl_2$ (3_1) and (4_1) occurs only via two-body decay while that of $CHFCl_2$ (5_1) via three-body decay as well. It appears that the onset of the three-body decay is observed when the combined energy of the vibrational excitation and photodissociating photon overcomes the dissociation barrier for it. In fact, this is the first time that three-body decay was observed in photodissociation of vibrationally excited molecules.

Another molecule that we studied is CH_3CFCl_2, where the about 235 or about 243 nm VMP of the second ($3\nu_{CH}$) and third ($4\nu_{CH}$) overtones of CH_3 was investigated. Figure 10 displays a representative PA spectrum and action spectra

of the photofragments as a function of the excitation laser wavelength scanned across the $3\nu_{CH}$ region. Figures 10(*a*), (*b*) and (*c*) include PA and H, ^{35}Cl and ^{37}Cl, and $^{35}Cl^*$ and $^{37}Cl^*$ action spectra respectively. The PA (10(*a*)) and H (10(*a*)) spectra reflect the contribution of all three CH_3CFCl_2 isotopomers ($CH_3CF^{35}Cl_2$ (natural abundance 57.05%), $CH_3CF^{35}Cl^{37}Cl$ (36.96%) and $CH_3CF^{37}Cl_2$ (5.99%)). The ^{35}Cl (10(*b*)) and $^{35}Cl^*$ (10(*c*)) action spectra account only for the two more abundant isotopomers, while the ^{37}Cl (10(*b*)) and $^{37}Cl^*$ (10(*c*)) action spectra account for the two less abundant isotopomers. Nevertheless, the action spectra of all photofragments exhibit a similar structure and the spectral features corresponding to the CH_3CFCl_2 isotopomers could not be distinguished under our resolution.

The jet-cooled action spectra differ from the corresponding room temperature PA spectrum, but both are characterized by multiple peak structures. In the action spectra most of the peaks are narrower and therefore more resolved. This is manifested by the appearance of two peaks in the low frequency end of the $3\nu_{CH}$ and $4\nu_{CH}$ manifolds compared with the one peak with a small shoulder observed in the PA spectra. Another prominent difference between the PA and action spectra is that the peak of highest frequency in the third overtone region is split into two peaks in the action spectra (figure 10). In this peak, contrary to the others, the overall contour width is almost similar to that in the PA spectrum.

Also, on the wave number axis of figure 10(*a*) a stick spectrum is shown. This spectrum is the result of a simplified LM model [131] employed by us [120] to assess the character of the prepared states. This model treated the three C-H stretches as equal and coupled via a 1:1 Darling–Dennison interaction. The deformation modes were treated as degenerate and the coupling between C-H stretches and deformations as Fermi type. From the model we obtained eigenvalues and eigenvectors consisting of different mixtures of stretches and deformations. The stick frequencies represent the eigenvalues, while the heights the of the eigenvectors' squared coefficients correspond to the contributions of the LM basis states where the energy is localized in a single C-H stretch (ZOBS). The heights do not necessarily represent the intensities, but rather demonstrate the extent of coupling of the C-H LM stretching states with the rest of the CH_3 stretch–deformation manifold. In view of the correspondence of the model to the experimental spectra, the observed states can be considered as different mixtures of methyl C-H stretches and deformations.

The linewidths of the overtone absorptions result from both homogeneous and inhomogeneous sources. Since the CH_3CFCl_2 molecule has 18 vibrational modes, of which eight have low energies, in the range of 241–926 cm^{-1}, at room temperature 57% of its population is in excited modes and it is anticipated that hot bands are underlying the overtone spectral regions and affect the PA spectra. Another contribution to the peak widths might be expected from the existence of several conformers. However, for CH_3CFCl_2 this possibility was ruled out since it possesses two conformers, staggered and eclipsed, where the eclipsed has 4.42 kcal mol^{-1} higher energy than the staggered, as found from Raman and IR spectra [132]. Because of the height of the barrier the probability of overcoming it at room temperature is very low, therefore the observed spectra apparently reflect only the staggered conformer. The action spectra of the jet-cooled CH_3CFCl_2 molecules were monitored at a rotational temperature of about 15 K and vibrational temperature of less than or equal to 100 K and the cooling eliminates most of the vibrational and some of the rotational congestion. Therefore, the peak widths in the action spectra,

still affected by the laser bandwidth and by some residual rotational and vibrational structure, are the upper limit of the homogeneous contribution.

The magnitude of the spectral splitting between the mixed states is related to the period of the vibrational energy oscillation between these states by $\Delta\nu = 1/c\tau$, while the time for IVR to the other modes of the molecule, is given by the homogeneous peak widths, $w = 1/2\pi c\tau$. The splittings in the second and third overtone manifolds, as measured from the jet-cooled action spectra, are in the range 25–60 cm^{-1}, corresponding to recurrence time estimates of 0.5–1.3 ps [120]. The peak widths range between 10 and 25 cm^{-1}, which means that concurrent with the oscillation the energy decays from the stretch–deformation mixed states to the quasicontinuum of states on a time-scale of at least 0.2–0.5 ps. Since the observed widths represent the upper limits for the homogeneous broadening, it is anticipated that the IVR to the rest of the molecule is even slower. Comparison of the oscillation periods in CH_3CFCl_2 and in the compounds with isolated CH chromophore, mentioned above, indicates that they are about one order of magnitude faster in the latter. These observations point to a weaker Fermi resonance in CH_3CFCl_2 than in compounds with isolated CH chromophore.

The two peaks that appear in the action spectra, compared with the one observed in the PA spectrum, at the high frequency end of the $4\nu_{CH}$ manifold (figure 10), are a result of a low-order resonance between the mixed state and a specific state that is in its vicinity. This is supported by the fact that contrary to most other peaks, where the PA linewidths are wider than in the action spectra, the width of the PA peak and of the contour in the action spectra are almost the same. A similar phenomenon was encountered for the ν_2 (symmetric C–H stretch) fundamental of this molecule, CH_3CFCl_2 [121].

The signal intensities obtained in the VMP of $3\nu_{CH}$ and $4\nu_{CH}$ of CH_3CFCl_2 relative to those obtained in about 235 or about 243 nm photodissociation of the vibrationless ground state reveal that the production of the atomic photofragments is significantly enhanced as a result of vibrational excitation. This enhancement can be due to the combined photon energies which are larger by about 8580 and about 11 270 cm^{-1} for $3\nu_{CH}$ and $4\nu_{CH}$ respectively, but also due to better FC factors. Moreover, the observed enhancement in the photodissociation stage is larger for $4\nu_{CH}$ than for $3\nu_{CH}$, possibly due to both the increase in energy and to a better FC overlap with the upper PESs. However, as for $CHFCl_2$, although C–H methyl stretches are excited, not only is C–H bond breaking enhanced, but large enhancements are obtained for both Cl and Cl* photofragments indicating that the energy flows into the C–Cl bond and leads to its effective cleavage.

The Cl*/Cl branching ratios for $3\nu_{CH}$ and $4\nu_{CH}$ VMP of CH_3CFCl_2 are comparable. However, they are twice that for 193 nm photodissociation although the combined energies in all three photodissociation processes are close. Moreover, the energy of the 193 nm photodissociation is between the combined energies employed in the $3\nu_{CH}$ and $4\nu_{CH}$ VMP, which leads to the conclusion that the vibrational pre-excitation itself causes the increase in the branching ratio. Support to the effect of the initial excitation on photoproducts yield can be also obtained from the H/[Cl + Cl*] branching ratio which rises upon excitation. Comparing the 235 nm direct photodissociation with the fundamental CH_3 symmetric stretch VMP revealed the same behaviour for Cl*/Cl and H/[Cl + Cl*] [121].

An increase in the branching into Cl* was also observed in VMP of CH_3Cl and CHD_2Cl [133] pre-excited to the fourth overtone of the C–H stretch, with a larger

increase in the CH_3Cl. Also, the photodissociation of vibrationally excited CF_3I (prepared by heating the sample) was found to increase the branching to the I products [134]. All these examples indicate that initial vibrational excitation of the alkyl group alters the branching ratio between the spin–orbit states of the ensuing halogen by affecting the photodissociation dynamics and leading to larger crossing between the involved surfaces.

4. Conclusions

The molecular systems described above highlight the competence of rovibrationally mediated photodissociation in realizing bond cleavage control by initial state preparation followed by interaction with a photodissociating photon. The comparison of action to absorption spectra, coupled with monitoring of the yield of different products, measurement of branching ratios, energy content and vectorial properties disclose the dynamical insights of the investigated processes. UV photodissociation of rovibrationally excited small molecules, comprising fundamental or overtones of pure stretches and entailing favourable FC factors that effectively promote them to the upper electronic states, where they become the reaction coordinate, results in selective bond breaking. In larger molecular systems, mixed states are excited, due to interactions between zero-order states, however, their character affects the subsequent interaction with photons. This results in different promotion to the upper electronic states even for neighbouring excited motions, or in different sampling of the upper states, enabling alteration of the dynamics while controlling the reaction and affecting the distribution or identity of the photoproducts. The obtained insights not only concern reaction control, but also provide new information regarding the energy flow pattern and the couplings of the prepared states. This is achieved by taking advantage of the narrowing in the jet-cooled action spectra, relative to the room temperature PA spectra, which enables observation of new features and determination of time-scale limits for vibrational redistribution. Since the field of reaction dynamics evolves toward studies of even larger molecular systems and it is attested that even preparation of mixed states impacts the photodissociation, it is essential to study larger molecules to test the impact of the VMP concept. Additional measurements accompanied by *ab initio* calculations of potential energy surfaces, which become feasible for larger molecules, should provide an excellent test ground for developing an increased understanding of how these processes occur. This insight will shed light on the interplay between nuclear and electronic motion underling photodissociation and hopefully reach an understanding that can be transferred from one molecular system to another. Whatever the outcome, one of the real gains in pursuing vibrationally mediated photodissociation will be the employment of its principles and methods to other fields.

Acknowledgements

This paper is dedicated to the memory of Peter Andresen (1945–2001), friend and colleague, a pioneer in the field of vibrationally mediated photodissociation.

We are indebted to many gifted graduate students and other collaborators that contributed to this work, and in particular to our colleagues, Professor P. J. Dagdigian, and Dr A. Melchior for reading the manuscript. Financial support from the Israeli Science Foundation (ISF) under grant No. 29/99-2, the United States–Israel Binational Foundation (BSF) under grant No. 1999044, the German–Israeli

Foundation (GIF) under grant No. I 0537-098.05/97 and the James Franck Binational German–Israeli Program in Laser–Matter Interaction for this research are also gratefully acknowledged.

References

[1] Levine, R. D., and Bernstein, R. B., 1987, *Molecular Reaction Dynamics and Chemical Reactivity* (Oxford: Oxford University Press).
[2] Schinke, R., 1993, *Photodissociation Dynamics* (Cambridge: Cambridge University Press).
[3] Butler, L. J., and Neumark, D. M., 1996, *J. phys. Chem.*, **110**, 12801.
[4] Dixon, R. N., 1994, *Chem. Soc. Rev.*, **23**, 375.
[5] Moore, C. B., and Smith, I. W. M., 1996, *J. phys. Chem.*, **100**, 12848.
[6] Bersohn, R., 1980, *IEEE. J. Quant. Electr.*, **QE-16**, 1208.
[7] Wayne, R. P., 1993, *J. geophys. Res.*, **98**, 13119.
[8] Ashfold, M. N. R., and Bagott, J. E., 1987, *Molecular Photodissociation Dynamics: Advances in Gas-phase Photochemistry and Kinetics* (London: Royal Society of Chemistry).
[9] Crim, F. F., 1996, *J. phys. Chem.*, **100**, 12725.
[10] Crim, F. F., 1993, *A. Rev. phys. Chem.*, **44**, 397.
[11] Crim, F. F., Hsiao, M. C., Scott, J. L., Sinha, A., and Vander Wal, R. L., 1990, *Phil. R. Soc. Lond. A.*, **332**, 259.
[12] Flynn, G. W., Parmenter, C. S., and Wodtke, A. M., 1996, *J. phys. Chem.*, **100**, 12817.
[13] Herzberg, G., 1966, *Molecular Spectra and Molecular Structure III. Electronic Spectra and Electronic Structure of Polyatomic Molecules* (Princeton, NJ: Van Nostrand); Herzberg, G. 1945, *Molecular Spectra and Molecular Structure II. Infrared and Raman Spectra of Polyatomic Molecules* (Princeton, NJ: Van Nostrand).
[14] Nesbitt, D. J., and Field, R. W., 1996, *J. phys. Chem.*, **110**, 12735.
[15] Lehmann, K. K., Scoles, G., and Pate, B. H., 1994, *A. Rev. phys. Chem.*, **45**, 241.
[16] Quack, M., and Kutzelnigg, W., 1995, *Ber. Bunsenges. phys. Chem.*, **99**, 231; Quack, M., 1990, *A. Rev. phys. Chem.*, **41**, 839.
[17] Bixon, M., and Jortner, J., 1968, *J. Chem. Phys.*, **48**, 715.
[18] Stannard, P. R., and Gelbart, W. M., 1981, *J. phys. Chem.*, **85**, 3592.
[19] Child, M. S., 1985, *Accts chem. Res.*, **18**, 45; Child, M. S., and Lawton, R. T. 1981, *J. chem. Soc., Faraday Discuss.*, **71**, 2731.
[20] Henry, B. R., 1977, *Accts chem. Res.*, **10**, 207.
[21] Mills, I. M., and Robiette, A. G., 1985, *Molec. Phys.*, **56**, 743.
[22] Valentini, J. J., 1987, *Laser Spectroscopy and its Applications*, Optical Engineering Vol. 11, edited by L. J. Radziemsky, R. W. Solarz, and J. A. Paisner, (New York: Marcel Dekker), p. 507; Valentini, J.J., 1985, *Spectroscopic Techniques*, Vol. 4, edited by G. A. Vanasse (New York: Academic Press), p. 1.
[23] Nibler, J. W., and Knighten, G. V., 1979, *Raman Spectroscopy of Gases and Liquids*, Topics in Applied Physics, Vol. 11, edited by A. Weber (Berlin: Springer-Verlag), p. 253.
[24] West, G. A., Barrett, J. J., Siebert, D. R., and Reddy, K. V., 1983, *Rev. scient. Instrum.*, **54**, 797.
[25] Hamilton, C. H., Kinsey, J. L., and Field, R. W., 1986, *A. Rev. phys. Chem.*, **37**, 493.
[26] Schultz, P. A., Sudbo, A. S., Krajnovich, D. J., Kwok, H. S., Shen, Y. R., and Lee, Y. T., 1979, *A. Rev. phys. Chem.*, **30**, 379.
[27] Bergmann, K., Theuer, H., and Shore, B. W., 1998, *Rev. mod. Phys.*, **70**, 1003.
[28] Pfab, J., 1995, *Spectroscopy in Environmental Sciences*, edited by R. J. H. Clark and R. E. Hester (New York: John Wiley), p. 149.
[29] Dieke, G. H., and Crosswhite, H. M. 1962, *J. Quantum Spectrosc. radiat. Transfer*, **2**, 97.

[30] Tonokura, K., Matsumi, Y., Kawasaki, M., Tasaki, S., and Bersohn, R., 1990, *J. chem. Phys.*, **93**, 7981; Matsumi, Y., Tonokura, K., Kawasaki, M., Tsuji, K., and Obi, K., 1993, *J. chem. Phys.*, **98**, 8330.
[31] Liyange, R., Yang, Y., Hashimoto, S., Gordon, R. J., and Field, R. W., 1995, *J. chem. Phys.*, **103**, 6811.
[32] Wiley, W. C., and McLaren, I. H., 1955, *Rev. scient Instrum.*, **26**, 1150.
[33] Zare, R. N., 1972, *Molec. Photochem.*, **4**, 1.
[34] Hall, G. E., and Houston, P. L., 1989, *A. Rev. phys. Chem.*, **40**, 375.
[35] Ashfold, M. N. R., Lambert, I. R., Mordaunt, D. H., Morley, G. P., and Western, C. M., 1992, *J. phys. Chem.*, **96**, 2938.
[36] Gordon, R. J., and Hall, G. E., 1996, *Adv. chem. Phys.*, **96**, 1.
[37] Barnes, R. J., Sinha, A., Dagdigian, P. J., and Lambert, H. M., 1999, *J. chem. Phys.*, **111**, 151.
[38] Beswick, J. A., Shapiro, M., and Sharon, R., 1977, *J. chem. Phys.*, **67**, 4045.
[39] Shapiro, M., 1977, *Chem. Phys. Lett.*, **46**, 442.
[40] Sheppard, M. G., and Walker, R. B., 1983, *J. chem. Phys.*, **78**, 7191.
[41] Zittel, P. F., and Little, D. D., 1980, *J. chem. Phys.*, **72**, 5900.
[42] Adler-Golden, S. M., Schweitzer, E. L., and Steinfeld, J. I., 1982, *J. chem. Phys.*, **76**, 2201.
[43] Zittel, P. F., Darnton, L. A., and Little, D. D., 1983, *J. chem. Phys.*, **79**, 5991; Zittel, P. F., and Masturzo, D. E., 1986, *J. Chem. Phys.*, **85**, 4362.
[44] Zittel, P. F., and Little, D. D., 1981, *Chem. Phys.*, **63**, 227.
[45] Joens, J. A., and Bair, E. J., 1983, *J. phys. Chem.*, **87**, 4613.
[46] Ticich, T. M., Likar, M. D., Dubal, H., Butler, L. J., and Crim, F. F., 1987, *J. chem. Phys.*, **87**, 5820; Butler, L. J., Ticich, T. M., Likar, M. D., and Crim, F. F., 1986, *J. chem. Phys.*, **85**, 233.
[47] Sinha, A., Vander Wal, R. L., and Crim, F. F., 1989, *J. chem. Phys.*, **91**, 2929.
[48] Likar, M. D., Baggott, J. E., and Crim, F. F., 1989, *J. chem. Phys.*, **90**, 6266.
[49] Schinke, R., Engel, V., Andresen, P., Hausler, D., and Balint-Kurti, G., 1985, *Phys. Rev. Lett.*, **55**, 1180; Hausler, D., Andresen, P., and Schinke, R., 1987, *J. chem. Phys.*, **87**, 3949.
[50] Segev, E., and Shapiro, M., 1982, *J. chem. Phys.*, **77**, 5604.
[51] Engel, V., and Schinke, R., 1988, *J. chem. Phys.*, **88**, 6831.
[52] Zhang, J., and Imre, D. G., 1988, *Chem. Phys. Lett.*, **149**, 233; Imre, D. G., and Zhang, J. 1989, *Chem. Phys.*, **139**, 89; Zhang, J., Imre, D. G., and Frederick, J. H., 1989, *J. phys. Chem.*, **93**, 1840.
[53] Sorbie, K. S., and Murrell, J. N., 1975, *Molec. Phys.*, **29**, 1387; Sorbie, K. S., and Murrell, J. N., 1976, *Molec. Phys.*, **31**, 905.
[54] Staemmler, V., and Palma, A., 1985, *Chem. Phys.*, **93**, 63.
[55] Vander Wal, R. L., Scott, J. L., and Crim, F. F., 1990, *J. chem. Phys.*, **92**, 803; Vander Wal, R. L., Scott, J. L., Crim, F. F., Weide, K., and Schinke, R., 1991, *J. chem. Phys.*, **94**, 3548.
[56] Bar, I., Cohen, Y., David, D., Rosenwaks, S., and Valentini, J. J., 1990, *J. chem. Phys.*, **93**, 2146; Bar, I., Cohen, Y., David, D., Arusi-Parpar, T., Rosenwaks, S., and Valentini, J. J., 1991, *J. chem. Phys.*, **95**, 3341.
[57] Cohen, Y., Bar, I., and Rosenwaks, S., 1995, *J. chem. Phys.*, **102**, 3612.
[58] Brouard, M., and Langford, S. R., 1997, *J. chem. Phys.*, **106**, 6354.
[59] Shafer, N., Satyapal, S., and Bersohn, R., 1989, *J. chem. Phys.*, **90**, 6807.
[60] Plusquellic, D. F., Votava, O., and Nesbitt, D. J., 1998, *J. chem. Phys.*, **109**, 6631.
[61] Schroder, T., Schinke, R., Ehara, M., and Yamashita, K., 1998, *J. chem. Phys.*, **109**, 6641.
[62] Engel, V., Staemmler, V., Vander Wal, R. L., Crim, F. F., Sension, R. J., Hudson, B., Andresen, P., Hennig, S., Weide, K., and Schinke, R., 1992, *J. phys. Chem.*, **96**, 3201.
[63] David, D., Strugano, A., Bar, I., and Rosenwaks, S., 1993, *J. chem. Phys.*, **98**, 409.
[64] Vander Wal, R. L., and Crim, F. F., 1989, *J. phys. Chem.*, **93**, 5331; Vander Wal, R. L., Scott, J. L., and Crim, F. F., 1991, *J. chem. Phys.*, **94**, 1859.

[65] Brouard, M., Langford, S. R., and Manolopoulos, D. E., 1994, *J. chem. Phys.*, **101**, 7458.
[66] Plusquellic, D. F., Votava, O., and Nesbitt, D. J. 1994, *J. chem. Phys.*, **101**, 6356.
[67] Cohen, Y., Bar, I., and Rosenwaks, S., 1994, *Chem. Phys. Lett.*, **228**, 426.
[68] David, D., Bar, I., and Rosenwaks, S., 1993, *J. chem. Phys.*, **99**, 4218; David, D., Bar, I., and Rosenwaks, S., 1993, *J. phys. Chem.*, **97**, 11571; Bar, I., David, D., and Rosenwaks, S., 1994, *Chem. Phys.,* **187**, 21; David, D., Bar, I., and Rosenwaks, S., 1994, *Photochem. Photobiol. A: Chem.*, **80**, 23.
[69] David, D., Strugano, A., Bar, I., and Rosenwaks, S., 1992, *Appl. Spectrosc.*, **46**, 1149.
[70] Herman, M., Lievin, J., Vander Auwera, J., and Campargue, A., 1999, *Adv. chem. Phys.*, **108**, 1.
[71] Child, M. S., and Halonen, L. 1984, *Adv. chem. Phys.*, **57**, 1; Zhan, X., and Halonen, L., 1993, *J. molec. Spectrosc.*, **160**, 464; Jungner P., and Halonen, L., 1997, *J. chem. Phys.*, **107**, 1680.
[72] Scherer, G. J., Lehmann, K. K., and Klemperer, W., 1983, *J. chem. Phys.*, **78**, 2817.
[73] Smith, B. C., and Winn, J. S., 1988, *J. chem. Phys.*, **89**, 4638; ibid., 1991, *J. chem. Phys.*, **94**, 4120.
[74] Bramley, M. J., Carter, S., Handy, N. C., and Mills, I. M., 1993, *J. molec. Spectrosc.*, **160**, 181.
[75] Abbouti Temsamani, M., and Herman, M., 1995, *J. chem. Phys.*, **102**, 6371; ibid., 1996, *J. chem. Phys.*, **105**, 1355; Herman, M., El Idrissi, M. I., Pisarchik, A., Campargue, A., Gaillot, A.-C., Biennier, L., Lonardo, G. D., and Fusina, L., 1998, *J. chem. Phys.*, **108**, 1377.
[76] Lievin, J., Abbouti Temsamani, M., Gaspard, P., and Herman, M., 1995, *Chem. Phys.*, **190**, 419; Pisarchik, A., Abbouti Temsamani, M., Vander Auwera, J., and Herman, M., 1993, *Chem. Phys. Lett.*, **206**, 343.
[77] Campargue, A., Abbouti Temsamani, M., and Herman, M., 1997, *Molec. Phys.*, **90**, 793; Campargue, A., Abbouti Temsamani, M., and Herman, M., 1997, *Molec. Phys.*, **90**, 807; Campargue, A., Biennier, L., and Herman, M., 1998, *Molec. Phys.*, **93**, 457.
[78] Abbouti Temsamani, M., Herman, M., Solina, S. A. B., O'Brien, J. P., and Field, R. W., 1996, *J. chem. Phys.*, **105**, 11357.
[79] Yamanouchi, K., Ikeda, N., Jonas, D. M., Lundberg, J. K., Adamson, G. W., and Field, R. W., 1991, *J. chem. Phys.*, **95**, 6330.
[80] Drucker, S., O'Brien, J. P., Patel, P., and Field, R. W., 1997, *J. chem. Phys.*, **106**, 3423; Solina, S. A. B., O'Brien, J. P., Field, R. W., and Polik, W. F., 1995, *Ber. Bunsenges. phys. Chem.*, **99**, 555; ibid., 1996, *J. phys. Chem.*, **100**, 7797; Jonas, D. M., Solina, S. A. B., Rajaram, B., Silbey, R. J., Field, R. W., Yamanouchi, K., and Tsuchiya, S., 1993, *J. chem. Phys.*, **99**, 7350.
[81] Utz, A. L., Carrasquillo, M., Tobiason, J. D., and Crim, F. F., 1995, *Chem. Phys.*, **190**, 311; Utz, A. L., Tobiason, J. D., Carrasquillo, M., Fritz, M. D., and Crim, F. F., 1992, *J. chem. Phys.*, **97**, 389.
[82] Chadwick, B. L., Milce, A. P., and Orr, B. J., 1994, *Can. J. Phys.*, **72**, 939; Payne, M. A., Milce, A. P., Frost, M. J., and Orr, B. J., 1997, *Chem. Phys. Lett.*, **265**, 244; Milce, A. P., and Orr, B. J., 1997, *J. chem. Phys.*, **106**, 3592; ibid., 1996, *J. chem. Phys.*, **104**, 6423; Orr, B. J., 1995, *Chem. Phys.*, **190**, 261.
[83] Wu, C. Y. R., Chien, T. S., Liu, G. S., Judge, D. L., and Caldwell, J. J., 1989, *J. chem. Phys.*, **91**, 272.
[84] Ingold, C. K., and King, G. W., 1953, *J. chem. Soc.*, **1953,** 2702.
[85] Innes, K. K., 1954, *J. chem. Phys.*, **22**, 863; Foo, P. D., and Innes, K. K., 1973, *Chem. Phys. Lett.*, **22**, 439.
[86] Osamura, Y., Mitsuhashi, F., and Iwata, S., 1989, *Chem. Phys. Lett.*, **164**, 205.
[87] Shi, Y., and Suzuki, T., 1998, *J. phys. Chem. A*, **102**, 7414; Suzuki, T., Shi, Y., and Kohguchi, H., 1997, *J. chem. Phys.*, **106**, 5292; Hashimoto, N., Yonekura, N., and Suzuki, T., 1997, *Chem. Phys. Lett.*, **264**, 545.
[88] Mourdaunt, D. H., Ashfold, M. N. R., Dixon, R. N., Loffler, P., Schnieder, L., and Welge, K. H., 1998, *J. chem. Phys.*, **108**, 519; Ashfold, M. N. R., Mourdaunt,

D. H., and Wilson, S. H. S., 1996, *Adv. Photochem.*, **21**, 217; Mourdaunt, D. H., and Ashfold, M. N. R., 1994, *J. chem. Phys.*, **101**, 2630.
[89] Balko, B. A., Zhang, J., and Lee, Y. T., 1991, *J. chem. Phys.*, **94**, 7958; Shiromaru, H., Achiba, Y., Kimura, K., and Lee, Y. T., 1987, *J. phys. Chem.*, **91**, 17; Wodtke, A. M., and Lee, Y. T., 1985, *J. phys. Chem.*, **89**, 4744.
[90] Wang, J.-H., Hsu, Y.-T., and Liu, K. 1997, *J. phys. Chem. A*, **101**, 6593.
[91] Loffler, P., Wrede, E., Schnieder, L., Halpern, J. B., Jackson, W. M., and Welge, K. H., 1998, *J. chem. Phys.*, **109**, 5231.
[92] Hsu, Y.-C., Chen, F.-T., Chou, L.-C., and Shiu, Y.-J., 1996, *J. chem. Phys.*, **105**, 9153.
[93] Cui, Q., Morokuma, K., and Stanton, J. F., 1996, *Chem. Phys. Lett*, **263**, 46; Cui, Q., and Morokuma, K., 1997, *Chem. Phys. Lett.*, **272**, 319.
[94] Schmid, R. P., Ganot, Y., Bar, I., and Rosenwaks, S., 1998, *J. chem. Phys.*, **109**, 8959; Arusi-Parpar, T., Schmid, R. P., and Ganot, Y., 1998, *Chem. Phys. Lett.*, **287**, 347; Schmid, R. P., Arusi-Parpar, T., Li, R.-J., Bar, I., and Rosenwaks, S., 1997, *J. chem. Phys.*, **107**, 385.
[95] Arusi-Parpar, T., Schmid, R. P., Li, R.-J., Bar, I., and Rosenwaks, S., 1997, *Chem. Phys. Lett.*, **268**, 163; Schmid, R. P., Ganot, Y., Rosenwaks, S., and Bar, I., 1999, *J. Molec. Struct.*, **480–481**, 197.
[96] Woods, E., Berghout, H. L., Cheatum, C. M., and Crim. F. F., 2000, *J. phys. Chem. A*, **104**, 10356.
[97] Go, J., Cronin, T. J., and Perry, D. S., 1993, *Chem. Phys.*, **175**, 127.
[98] Gambogi, J. E., Kerstel, E. R. Th., Lehmann, K. K., and Scoles, G., 1994, *J. chem. Phys.*, **100**, 2612; McIlroy, A., Nesbitt, D. J., Kerstel, E. R. Th., Pate, B. H., Lehmann, K. K., and Scoles, G., 1994, *J. chem. Phys.*, **100**, 2596.
[99] Baylor, L. C., Weitz, E., and Hofmann, P., 1989, *J. chem. Phys.*, **90**, 615; Hofmann, P., Gerber, R. B., Ratner, M. A., Baylor, L. C., and Weitz, E., 1988, *J. chem. Phys.*, **88**, 7434.
[100] Crofton, M. W., Stevens, C. G., Klenerman, D., Gutow, J. H., and Zare, R. N., 1988, *J. chem. Phys.*, **89**, 7100.
[101] Campargue, A., Biennier, L., Gamache, A., Kachanov, A., Romainin, D., and Herman, M., 1999, *J. chem. Phys.*, **111**, 7888.
[102] Satyapal, S., and Bersohn, R., 1991, *J. phys. Chem.*, **95**, 8004.
[103] Seki, K., and Okabe, H., 1992, *J. phys. Chem.*, **96**, 3345.
[104] Ni, C.-K., Huang, J. D., Chen, Y. T., Kung, A. H., and Jackson, W. M., 1999, *J. chem. Phys.*, **110**, 3320.
[105] Sun, W., Yokoyama, K., Robinson, J. C., Suits, A. G., and Neumark, D. M., 1999, *J. chem. Phys.*, **110**, 4363.
[106] Mebel, A. M., Jackson, W. M., Chang, A. H. H., and Lin, S. H., 1998, *J. Am. Chem. Soc.*, **120**, 5751.
[107] Chen, X., Ganot, Y., Bar, I., and Rosenwaks, S., 2000, *J. chem. Phys.*, **113**, 5134.
[108] Ichimura, T., Kirk, A. W., and Tschuikow-Roux, E., 1977, *J. phys. Chem.*, **81**, 2040; Ichimura, T., Kirk, A. W., and Tschuikow-Roux, E., 1977, *Int. J. chem. Kinetics*, **9**, 697.
[109] Rebbert, R. E., Lias, S. G., and Ausloos, P., 1978, *J. Photochem.*, **8**, 17.
[110] Yang, X., Felder, P., and Huber, J. R., 1994, *Chem. Phys.*, **189**, 124.
[111] Melchior, A., Knupfer, P., Bar, I., Rosenwaks, S., Laurent, T., Volpp, H.-R., and Wolfrum, J., 1996, *J. phys. Chem.*, **100**, 13375; Melchior, A., Bar, I., and Rosenwaks, S., 1997., *J. chem. Phys.*, **107**, 8476; Melchior, A., Lambert, H. M., Dagdigian, P. J., Bar, I., and Rosenwaks, S., 1997, *Israel J. Chem.*, **37**, 455.
[112] Brownsword, R. A., Hillenkamp, M., Laurent, T., Vatsa, R. K., Volpp, H.-R., and Wolfrum, J., 1997, *J. phys. Chem. A*, **101**, 995; Brownsword, R. A., Hillenkamp, M., Laurent, T., Volpp, H.-R., Wolfrum, J., Vatsa, R. K., and Yoo, H.-S., 1997, *J. chem. Phys.*, **107**, 779; Brownsword, R. A., Schmiechen, P., Volpp, H.-R., Upadhyaya, H. P., Jung, Y. J., and Jung, K.-H., 1999, *J. chem. Phys.*, **110**, 11823.
[113] Lai, L.-H., Hsu, Y.-T., and Liu, K., 1999, *Chem. Phys. Lett.*, **307**, 385.

[114] LAMBERT, H. M., DAGDIGIAN, P. J., and ALEXANDER, M. H., 1998, *J. chem. Phys.*, **108**, 4460.
[115] ALEXANDER, M. H., POUILLY, B., and DUHOO, T., 1993, *J. chem. Phys.*, **99**, 1752.
[116] ZHANG, J., DULLIGAN, M., and WITTIG, C., 1997, *J. chem. Phys.*, **107**, 1403.
[117] KAWASAKI, M., SUTO, K., SATO, Y., MATSUMI, Y., and BERSOHN, R. 1996, *J. phys. Chem.*, **100**, 19853.
[118] REGAN, P. M., ASCENZI, D., BROWN, A., BALINT-KURTI, G. G., and ORR-EWING, A. J., 2000, *J. chem. Phys.*, **112**, 10259.
[119] REGAN, P. M., LANGFORD, S. R., ASCENZI, D., COOK, P. A., ORR-EWING, A. J., and ASHFOLD, M. N. R., 1999, *Phys. Chem. chem. Phys.*, **1**, 3247.
[120] MELCHIOR, A., CHEN, X., BAR, I., and ROSENWAKS, S., 2000, *J. phys. Chem.*, **104**, 7927; CHEN, X., MAROM, R., ROSENWAKS, S., BAR, I., EINFELD, T., MAUL, C., and GERICKE, K.-H., 2001, *J. chem. Phys.*, **114**, 9033.
[121] MELCHIOR, A., CHEN, X., BAR, I., and ROSENWAKS, S., 2000, *J. chem. Phys.*, **112**, 10787; MELCHIOR, A., CHEN, X., BAR, I., and ROSENWAKS, S., 2000, *J. chem. Phys.*, **112**, 4111; MELCHIOR, A., CHEN, X., BAR, I., and ROSENWAKS, S., 2000, *Chem. Phys. Lett.*, **315**, 421.
[122] DUBAL, H.-R., and QUACK, M., 1984, *Molec. Phys.*, **53**, 257.
[123] BALDACCI, A., PASSERINI, A., and GHERSETTI, S., 1984, *Spectrochim. Acta*, **40A**, 1.
[124] SNELS, M., and QUACK, M., 1991. *J. chem. Phys.*, **95**, 6355.
[125] HIPPLER, M., and QUACK, M., 1996, *J. chem. Phys.*, **104**, 7426.
[126] BOYARKIN O. V., and RIZZO, T. R., 1996, *J. chem. Phys.*, **105**, 6285; BOYARKIN, O. V., SETTLE, R. D. F., and RIZZO, T. R., 1995, *Ber. Bunsenges. phys. Chem.*, **99**, 504.
[127] ROBIN, M. B., 1985, *Can. J. Chem.*, **63**, 2032.
[128] OKABE, H., 1978, *Photodissociation of Small Molecules* (New York: John Wiley).
[129] MAUL, C., and GERICKE, K.-H., 2000, *J. phys. Chem. A*, **104**, 2531; MAUL, C., and GERICKE, K.-H., 1997, *Int. Rev. Phys. Chem.*, **16**, 1.
[130] YING, J. F., and LEUNG, K. T., 1996, *J. chem. Phys.*, **105**, 2188.
[131] DUNCAN, J. L., NEW, C. A., and LEAVITT, B., 1995, *J. chem. Phys.*, **102**, 4012.
[132] DURIG, J. R., WURREY, C. J., BUCY, W. E., and SLOAN, A. E., 1976, *Spectrochim. Acta*, **32A**, 175.
[133] LAMBERT, H. M., and DAGDIGIAN, P. J., 1997, *Chem. Phys. Lett.*, **275**, 499; LAMBERT, H. M., and DAGDIGIAN, P. J., 1998, *J. chem. Phys.*, **109**, 781.
[134] PERSON, M. D., KASH, P. W., and BUTLER, L. J., 1991, *J. chem. Phys.*, **94**, 2557.